A physically based model to predict hydraulic erosion of fine-grained riverbanks: The role of form roughness in limiting erosion

Stephen E. Darby,[1] Hai Q. Trieu,[1] Paul A. Carling,[1] Juha Sarkkula,[2] Jorma Koponen,[3] Matti Kummu,[4] Iwona Conlan,[5] and Julian Leyland[1]

[1]   Hydraulic erosion of bank toe materials is the dominant factor controlling the long-term rate of riverbank retreat. In principle, hydraulic bank erosion can be quantified using an excess shear stress model, but difficulties in estimating input parameters seriously inhibit the predictive accuracy of this approach. Herein a combination of analytical modeling and novel field measurement techniques is employed to improve the parameterization of an excess shear stress model as applied to the Lower Mekong River. Boundary shear stress is estimated using a model (Kean and Smith, 2006a, 2006b) for flow over the irregular bank topography that is characteristic of fine-grained riverbanks. Bank erodibility parameters were obtained using a cohesive strength meter (Tolhurst et al., 1999). The new model was used to estimate annual bank erosion rates via integration across the Mekong's annual flow regime. Importantly, the simulations represent the first predictions of hydraulic bank erosion that do not require recourse to calibration, thereby providing a stronger physical basis for the simulation of bank erosion. Model predictions, as evaluated by comparing simulated annual rates of bank toe retreat with estimates of bank retreat derived from analysis of aerial photographs and satellite imagery, indicate a tendency to overpredict erosion (root-mean-square error equals ±0.53 m/yr). Form roughness induced by bank topographic features is shown to be a major component (61%–85%) of the spatially averaged total shear stress, and as such it can be viewed as an important factor that self-limits bank erosion.

1.   Introduction

[2]   The erosion of sediment from riverbanks is a key factor affecting a range of physical, ecological and management issues in the fluvial environment, with significant fractions of the total sediment load transported within alluvial sedimentary systems being sourced from river bank erosion [*Rinaldi and Darby*, 2007]. When rivers flow through densely populated regions, even modest rates of bank erosion can present a significant hazard to agriculture, built infrastructure and navigation. Furthermore, the sediments supplied from the process can be important in the establishment of river and floodplain morphology and their associated habitats [*Thorne and Lewin*, 1979; *Millar*, 2000; *Goodson et al.*, 2002; *Eaton et al.*, 2004], as well as contributing to the loss of channel conveyance [*Piégay et al.*, 2005] and nutrient or contaminant problems [e.g., *Marron*, 1992; *Reneau et al.*, 2004] downstream. For all these reasons an ability to predict bank erosion rates accurately is fundamentally important in fluvial geomorphology and hydraulic engineering.

[3]   Given the importance of the topic, bank erosion has been the subject of a large body of research. Recent work has focused on developing models to predict the conditions under which riverbanks become susceptible to large-scale mass failure under gravity [e.g., *Osman and Thorne*, 1988; *Simon and Collison*, 2002; *Rinaldi and Casagli*, 1999; *Rinaldi et al.*, 2004], but fewer studies have been concerned with the process of hydraulic (also known as fluvial) erosion, which involves the removal of bank materials by the direct erosive action of the flow. This is a significant limitation because mass wasting is often triggered by hydraulically controlled bank toe erosion, and it is widely accepted that the long-term rate of bank retreat is, therefore, controlled by the rate of hydraulic erosion at the toe [*Thorne*, 1982;

[1]School of Geography, University of Southampton, Highfield, Southampton, UK.
[2]Finnish Environment Institute, Helsinki, Finland.
[3]Environmental Impact Assessment Centre of Finland Ltd, Espoo, Finland.
[4]Water and Development Research Group, Aalto University School of Science and Technology (TKK), Aalto University, Espoo, Finland.
[5]Department of Resource Management and Geography, University of Melbourne, Melbourne, Victoria, Australia.

Figure 1. Location of study sites within the Lower Mekong River Basin. Google Earth images show the local context for the study sites at Ang Nyay, Ban Hom, Friendship Bridge, and Pakse. The locations of bank material sampling sites (see text for latitudes and longitudes) are indicated by the open circles. Google Earth imagery ©Google Inc. Used with permission.

Rinaldi and Darby, 2007]. Hydraulic bank erosion rates are most commonly quantified using an excess shear stress formula such as [*Partheniades*, 1965; *Arulanandan et al.*, 1980]

$$\varepsilon = k\left(\tau_{sf} - \tau_c\right)^a, \qquad (1)$$

where ε (m/s) is the fluvial bank erosion rate per unit time and unit bank area, τ_{sf} (Pa) is the skin drag component of boundary shear stress, k (m^2 s/kg) and τ_c (Pa) are erodibility parameters (coefficient, k, and critical shear stress, τ_c) and a (dimensionless) is an empirically derived exponent, often assumed to take a value of 1 in bank erosion studies [*Rinaldi and Darby*, 2007].

[4] Excess shear stress models of this type have been used in a range of geomorphological applications [e.g., *Govers*, 1991; *Howard*, 1994; *Arulanandan et al.*, 1980]. These models have the great advantage of simplicity, but observed rates of bank erosion range over several orders of magnitude [*Hooke*, 1980] and bank erosion rates are predictable only to the extent that the controlling parameters can be estimated accurately. Unfortunately, characterizing these parameters accurately is challenging, due to the very high natural variability of bank materials [*Darby*, 1998; *Rinaldi and Darby*, 2007]. Moreover, an issue that has been overlooked frequently is the need to partition the boundary shear stress exerted on eroding riverbanks into skin drag and form drag components, the former being the stress available for bank erosion. The few empirical and numerical studies that have investigated near bank flows confirm the dominance of the form drag component [*Thorne and Furbish*, 1995; *McBride et al.*, 2007], but the inherent complexity of flow over the irregular topography characteristic of eroding riverbanks has until recently inhibited analytical solutions. For these several reasons, applications of excess shear stress models frequently involve predictive errors of up to an order of magnitude [*Darby*, 1998; *Mosselman*, 1998; *Julian and Torres*, 2006]. In light of this difficulty, researchers often simply estimate the erodibility parameter values in equation (1) by means of calibration, even though this diminishes the physical basis of the model [*Julian and Torres*, 2006; *Constantine et al.*, 2009].

[5] To address these issues, recent advances in measurement and modeling technologies are exploited herein in an attempt to improve the parameterization of the excess shear stress model. Specifically, a jet testing device is employed to characterize the erodibility of fine-grained bank sediments, while a hydraulic model is used to partition the skin drag and form drag components of boundary shear stress exerted on eroding banks. The analytical nature of this hydraulic model is significant, since the need for computationally intensive numerical simulation is avoided. Moreover, using these new techniques enables parameterization of the excess shear stress model without recourse to calibration, thereby providing a stronger physical basis for the simulation of bank erosion. Not only are all relevant input parameters readily measurable but, as shown below, they can be linked to flow discharge records commonly available at stream gauging stations, enabling convenient simulation of high-resolution, multidecadal, time series of bank erosion.

2. Study Site

[6] The Mekong River is a globally significant watercourse, ranking 27th in terms of its basin area (816,000 km^2) [*Kummu*, 2008] and, at approximately 4900 km [*Liu et al.*, 2007], it is the world's 12th longest river. The tropical monsoonal climate generates a mean annual runoff of 475 km^3 [*Mekong River Commission*, 2005] and a mean annual sediment load of 1.6×10^8 t [*Milliman and Meade*, 1983], values that rank 10th and 9th, respectively, among the world's rivers. Rising in Tibet and discharging into the South China Sea, the Mekong basin (Figure 1) can be divided into two units: (1) the Upper Mekong Basin, which lies within China, and (2) the Lower Mekong Basin (LMB) which lies to the south of the border between China and Laos. This division demarks the rapid broadening of basin form as it debouches from the confines of the Himalayas, prior to being joined by numerous, sizable tributaries [*Carling*, 2009a].
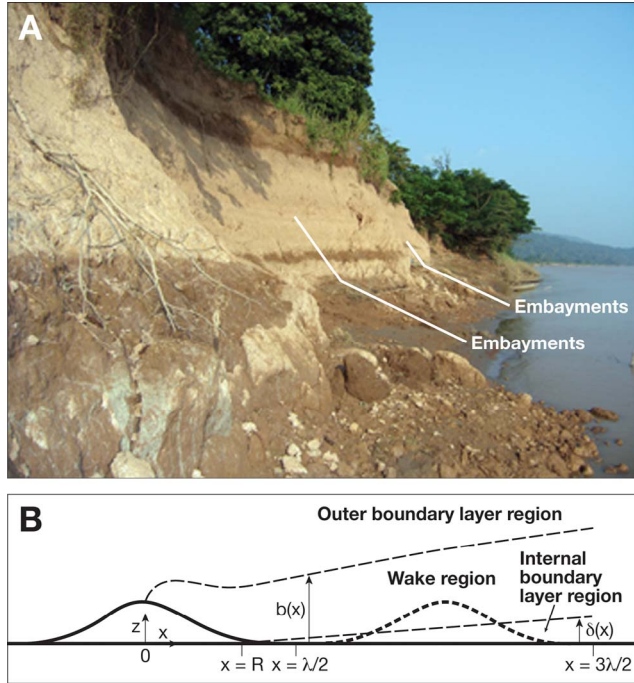
Figure 2. (a) Photograph of the riverbank at the Ban Hom study site on the Lower Mekong River illustrating the bank protruding into the flow between embayments. (b) Overview of the Gaussian-shaped plan view geometry of the modeled bank topographic roughness elements, along with the internal boundary layer, wake, and outer regions of the flow (flow direction is left to right). The thick dashed line of the downstream element denotes that it is removed from the flow, with the u_{ref}^2 for this element being the average squared velocity over this area. The unit "cell" from $\lambda/2$ to $3\lambda/2$ is the length over which the stresses are averaged. Figure 2b is reproduced from *Kean and Smith* [2006a, Figure 5].

[7] In this study we focus on four study sites on the Mekong main stem in Laos (Figure 1). Three of these, at Ang Nyay (18°3′15.9″N 102°19′5.5″E), Ban Hom (17°49′49″N 102°38′41″E) and Friendship Bridge (17°52′59″N 102°42′59″E), are located on the left bank within a reach that encompasses the gauging station at Vientiane. The fourth site is located further downstream, on the right bank close to the Pakse gauging station at 15°5′55″N 105°47′58″E. These sites are all located within single-thread or divided sinuous channels. The reach near Vientiane has an average gradient of about 1.0×10^{-4}, widths that range between 800 and 1300 m, and seasonal flow stage changes of around 13 m [*Carling*, 2009b; *Gupta and Liew*, 2007]. At Pakse, the channel is flatter (6.0×10^{-5}) and wider (typically ~2 km), with seasonal flow stage changes of about 14 m [*Carling*, 2009b; *Gupta and Liew*, 2007]. Much of the Mekong between Ang Nyay and Pakse is alluvial, with a fine sand bed and silty riverbanks that veneer patchy outcrops of bedrock. The presence of bedrock acts to constrain the lateral migration of the river, and alluvial bank erosion rates are typically rather low (~1 m/yr) [see *Kummu et al.*, 2008], despite the large scale of the river. A key feature of the river in this reach is its tendency to develop a divided channel (wandering) configuration, with large elongate islands. Thus, even if rates are low, it is clear that within the alluvial reaches the channel is actively migrating laterally via long-radius bends [*Carling*, 2009b].

[8] Prior studies of bank erosion have tended to be located within relatively small-scale upland or piedmont systems in humid temperate regions that often have low bank heights and coarse basal sediments (see *Rinaldi and Darby* [2007] for a review). In contrast, the riverbanks of the Mekong are high and, with the exception of isolated lenses of coarse material, composed of fine-grained, cohesive, sediments. For example, bank heights typically exceed 10 m, with sediments composed of reddish-brown sandy silts and/or gray clays. Furthermore, the LMB experiences a tropical monsoonal climate [*Mekong River Commission*, 2005]. River flows are therefore highly variable, with a prolonged annual flood (usually between June and November) and pronounced dry season (December to May) low flows. At Vientiane (mean annual flow of 4500 m³/s), flow discharge varies between about 1000 m³/s and a mean annual peak of 16,750 m³/s. Further downstream, at Pakse, substantially increased flows range between about 1700 m³/s to mean annual peaks of 37,700 m³/s (mean annual flow is 9860 m³/s). The hydrological context for this study is therefore relatively unusual in relation to prior studies, but the monsoonal flow regime is also convenient in the sense that it presents a relatively simple case in which it is feasible to model multi-decadal time series, each annual flood presenting a potentially erosive, but nevertheless individual, flow event.

3. Model Development

[9] In this paper two novel methods are applied to parameterize the terms in equation (1). Specifically, the *Kean and Smith* [2006a, 2006b] model is employed to estimate the skin drag component of bank boundary shear stress, while a jet testing device is used to estimate the erodibility of the riverbank materials. The use of these methods provides a means to obtain the very first predictions of hydraulic bank erosion rates that do not require recourse to calibration, thereby significantly enhancing the physical basis of the model relative to prior studies. Each of the two methods is now discussed.

3.1. Parameterization of Bank Shear Stress

[10] Near-bank flows are characterized by strong lateral shear and high form resistance induced by the topographic irregularities associated with eroding banks [e.g., *Thorne and Furbish*, 1995; *Kean and Smith*, 2006a]. In this paper *Kean and Smith*'s [2006a, 2006b] method of partitioning the drag on bank roughness elements into form and skin components is employed, in which

$$\tau_T = \tau_{sf} + \tau_d, \qquad (2)$$

where τ_T is the total shear stress on the boundary of the channel, τ_{sf} is the skin drag component and τ_d is the form drag component induced as a result of pressure forces acting on the surfaces of large-scale topographic elements (Figure 2a) which protrude into the flow. Note that, from

equation (1), it is the skin drag component that is of interest in the context of bank erosion modeling. Because prior models of riverbank erosion do not adequately incorporate the form drag component, use of the Kean and Smith model represents a potentially significant advance.

[11] The form drag (F) on an individual roughness element is defined as [*Kean and Smith*, 2006a]

$$F = \frac{1}{2} \rho C_D H B u_{ref}^2, \qquad (3)$$

where ρ is the density of water, H is the protrusion height of the element (this height being normal to the x axis in Figure 2b), B is the length of the direction perpendicular to the x and z axes defined in Figure 2b, u_{ref} is a reference velocity, and C_D is the drag coefficient of the element. In equation (3), the square of the reference velocity is defined by Kean and Smith as the average of the square of the velocity that would be present at the location of a roughness element if that element were removed from the flow. For each topographic element in a sequence of regularly spaced elements, the reference velocity is controlled by wakes shed from the element upstream [*Kean and Smith*, 2006a]. In addition, Figure 2b shows that u_{ref} is also affected by a growing internal boundary layer on the wall that begins at the reattachment point (R) of the separation zone on the upstream form. Consequently u_{ref} is affected by three interdependent regions: an internal boundary layer region, a wake region, and an outer boundary layer region and to calculate u_{ref}, the velocity field within each region must be determined.

[12] *Kean and Smith*'s [2006a] model follows *Smith and McLean* [1977] and *McLean and Smith* [1986] in describing the velocity field in each region separately, joining them together using matching conditions so that u_{ref} can be determined by spatially averaging the (matched) velocity field over the unit volume of the roughness element. This requires an assumption to be made about the element's geometry and, in Kean and Smith's analysis, the elements are approximated as Gaussian-shaped "bumps." *Kean and Smith* [2005, 2006b] provide data from small streams in the midwest and western United States to support this assumption, and the bank roughness elements at the Lower Mekong field sites in this study are also well described as Gaussian forms (see section 3.1.1). Regarding the methods employed to estimate the velocity field, within the internal boundary layer region the velocity is defined by the law of the wall [*Kean and Smith*, 2006a],

$$u = \frac{u_{*IBL}}{\kappa} \ln \frac{z}{z_{oSF}}, \qquad (4)$$

where κ is von Karman's constant, z is the distance away from the boundary, z_{oSF} is the local roughness height of the boundary without topographic roughness elements (i.e., a skin roughness height, see below for details), and u_{*IBL} is the shear velocity within the internal boundary layer (equals $\sqrt{\tau_{sf}/\rho}$). The flow in the outer region similarly follows the law of the wall,

$$u = \frac{u_{*T}}{\kappa} \ln \frac{z}{z_{oT}}, \qquad (5)$$

where $u_{*T} = \sqrt{\tau_T/\rho}$ and z_{oT} is the roughness height due to skin friction plus form drag. The wake region is modeled using *Schlichting*'s [1979] far-field wake solution,

$$u = u_b \left[1 - g(x) f\left(\frac{z - \eta}{b}\right)\right], \qquad (6)$$

within which *Kean and Smith* [2006a] employ

$$g(x) = A_2 \left(\frac{x + x_o}{C_D H}\right) \qquad (7)$$

and

$$f\left(\frac{z - \eta}{b}\right) = \left[1 - \left(\frac{z - \eta}{b}\right)^{3/2}\right]^2, \qquad (8)$$

where x is the distance downstream from the center of the element producing the wake, z is the distance away from the reference level of the roughness elements, $z = \eta$ is the surface of the boundary, u_b is the velocity at the top of the wake, x_o is the virtual origin, which Kean and Smith equate to zero, and the wake thickness, b (Figure 2), is given by [*Kean and Smith*, 2006a]

$$b = 2 A_1 C_D H \left(\frac{x + x_o}{C_D H}\right)^{1/2}. \qquad (9)$$

The constants A_1 and A_2 are set equal to $\sqrt{10\beta}$ and $\sqrt{20}/(18\beta)$, respectively, with β an empirically determined constant that sets the value of the eddy viscosity within the wake. *Kean and Smith* [2006a] used data from the flume experiments of *Hopson* [1999] to suggest

$$\beta = 0.226 \left[1 - \exp\left(-0.353 \frac{\lambda}{H}\right)\right], \qquad (10)$$

where λ is the spacing of the roughness elements.

[13] A critical aspect of the Kean and Smith model lies in applying the velocity matching conditions between the internal boundary layer and wake, and between the wake and the outer flow region. Full details of both matching conditions are reported in *Kean and Smith* [2006a] and are not repeated here for reasons of space. Suffice to note that equations (4), (5) and (6), together with the corresponding velocity matching conditions, fully specify the velocity field, $u(x, z)$, that would be present if the roughness element were removed from the flow. This procedure enables the reference velocity in equation (2) to be defined using [*Kean and Smith*, 2006a]

$$u_{ref}^2 = \frac{1}{A} \int_A u^2(x, z) dA, \qquad (11)$$

where A is the plan view area of the roughness element. For bank roughness elements that are Gaussian in shape, it follows that

$$A = H \sigma \sqrt{\pi/2} \left[erf\left(\frac{x_{dn} - x_c}{\sqrt{2}\sigma}\right) - erf\left(\frac{x_{up} - x_c}{\sqrt{2}\sigma}\right)\right], \qquad (12)$$

where σ is the streamwise length of the element, x is the streamwise coordinate, and the subscripts up, dn and c
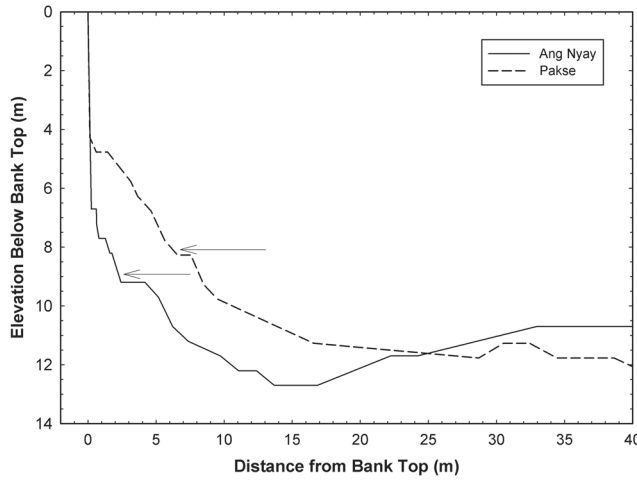
Figure 3. Examples of bank profiles at Ang Nyay and Pakse study sites, indicating that the longitudinal bank roughness profiles were collected from points (locations indicated by arrows) representative of the lower portion of the bank profile.

denote the upstream and downstream limits and crest of the roughness element.

[14] To close the model, a known value of velocity within the outer region of the flow must be specified (see below for details of how the outer region flow velocities are determined in this study), which then enables the total drag on the topographic elements to be related to properties of the outer flow via equation (1). Using (3), and recalling that the bank topographic roughness elements are assumed to be Gaussian in shape, the drag stress is calculated using

$$\tau_d = \frac{1}{2}\rho C_D \frac{H}{\lambda} u_{ref}^2, \tag{13}$$

By expressing the average skin friction stress in terms of the shear velocity in the internal boundary layer, the total stress on the boundary is written

$$\tau_T = \rho \langle u_{*IBL} \rangle^2 + \frac{1}{2}\rho C_D \frac{H}{\lambda} u_{ref}^2, \tag{14}$$

wherein *Kean and Smith* [2006a] estimate the drag coefficient using an empirical function derived from the experimental data of *Hopson* [1999],

$$C_D = 1.79 \exp\left(-0.77\frac{\sigma}{H}\right). \tag{15}$$

[15] To solve (14), initial estimates of the total roughness height and shear velocity, z_{oT} and u_{*T}, in the outer flow are made that match the specified outer velocity, u_{out}. This estimation procedure then enables $< u_{*IBL} >$ and u_{ref} to be determined via the velocity matching conditions and (11), from which improved estimates of u_{*T} and z_{oT} are obtained from (14) and (5). This iterative sequence is repeated until the solution converges. Input data requirements include a set of parameters describing the geometrical characteristics of the bank roughness elements (H, σ, λ), an estimate of the

roughness height associated with the skin drag component (z_{oSF}), and a specified flow velocity within the outer flow region, u_{out}, at a known distance from the boundary, z_{crit}. Details of how these parameters were estimated are provided below.

3.1.1. Parameterization of Bank Roughness Parameters

[16] At each study site, streamwise profiles of bank surface topography were obtained using a handheld Leica Disto A5 laser range finder (accuracy ±2 mm) to measure offsets at approximately periodic (0.5–1.0 m) intervals along survey transect lines positioned at constant elevations along the bank. Similar to the examples shown in *Kean and Smith* [2006a], the bank topographic features identified in this study are essentially two-dimensional; that is their shape does not significantly vary with elevation above the bed. At each site the longitudinal bank profiles were, therefore, positioned close to the base of the near-vertical face that is a ubiquitous feature of the Mekong's riverbanks (Figure 3). The survey transect is, therefore, in all cases representative of the lower portion of the bank, though the precise elevation of each transect above the bank toe varied in position between about 0.1 (Ang Nyay) and 0.5 (Pakse) of the bank height (Figure 3).

[17] For reasons of space, only one example (Figure 4) of the bank topographic profiles, from the Ang Nyay study site, is presented here. In all cases the length of an individual profile was sufficient to encompass a sequence of several bank roughness elements (see Table 1 for details). Following *Kean and Smith* [2005], each topographic profile initially was detrended to remove low-frequency undulations associated with channel curvature. The positions of higher-frequency undulations associated with individual roughness elements along the bank then were identified manually, prior to Gaussian curves being fitted to each of the individual "bumps" using Matlab's curve fitting toolbox. For all bumps in this study (126 bumps) statistically significant (P < 0.001) fits were obtained, with correlation coefficients ranging between 0.203 (with only five bumps having r^2 values less than 0.500) to 1.0 ($\mu = 0.833$, $\sigma = 0.142$). This indicates that the bank roughness elements are approximated well as Gaussian shapes, as has been found previously on a wide range of other riverbanks [*Kean and Smith*, 2006a, 2006b]. Note that, here and throughout this study, where parametric statistical tests are used, the data were scrutinized to ensure that underlying assumptions of the tests were not violated, and unless otherwise stated no such violations were found.

[18] Figure 4 is typical in that bank roughness elements are invariably irregularly shaped. *Kean and Smith* [2006b] show that the topography of irregular surfaces can be transformed into an equivalently rough surface of regularly spaced, identical, elements using the approximation

$$\begin{aligned} H_{reg} &= H_{88} \\ \sigma_{reg} &= \sigma_{88} \quad, \\ \lambda_{reg} &= 6H_{88} \end{aligned} \tag{17}$$

where the subscripts indicate the percentile of the extracted (irregular) bank roughness parameter distributions used to represent the equivalent "regularized" surface. The skin roughness height parameter, z_{oSF}, also was estimated using the bank topographic profiles. *Kean and Smith* [2005] suggest that finer scales of bank roughness can be characterized by
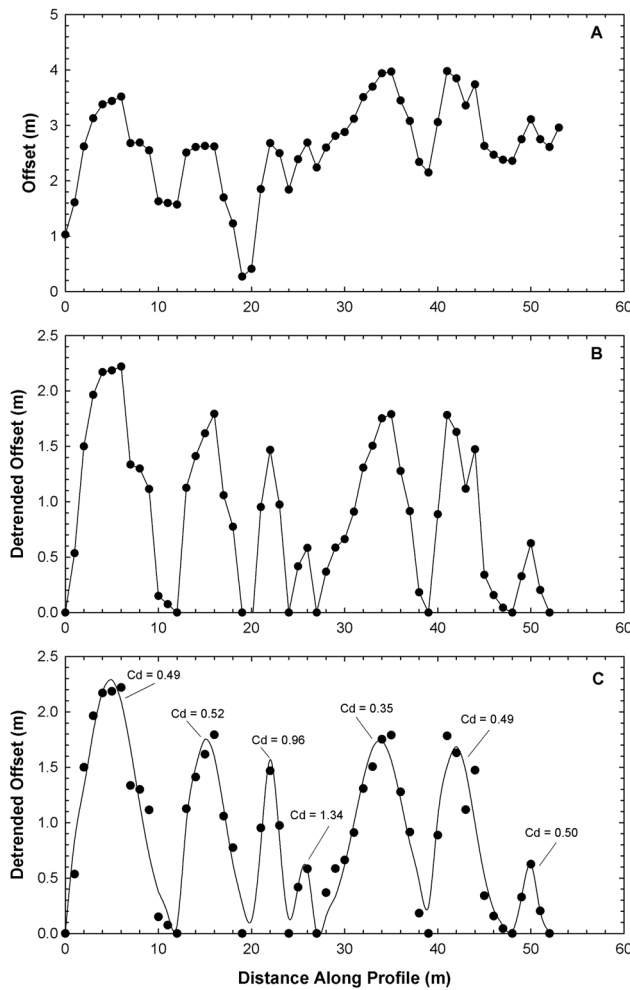
Figure 4. Measurements and analysis of part of the bank topographic profile from the Ang Nyay study site on the Lower Mekong River. (a) Original measurements with low-frequency undulations. (b) Detrended profile with low-frequency undulations removed. (c) Gaussian fits to the detrended sequence of topographic roughness elements. The drag coefficients (C_D) associated with each of the fitted bumps are also shown. Note change of vertical scale in Figure 4a relative to Figures 4b and 4c.

Figure 5. Characterization of the finer scale of bank roughness at the Ang Nyay study site on the Lower Mekong River. (a) Deviations from the Gaussian fits shown in Figure 3c. (b) Power spectrum of the deviations showing the lack of a statistically significant characteristic frequency, the 0.05 and 0.01 significance levels being illustrated by the solid and dashed gray horizontal lines, respectively.

analyzing the deviations from the Gaussian fits (Figure 5a). Specifically, Fourier analysis is used to identify any characteristic wavelengths associated with this secondary roughness and, if significant, it can be modeled as a series of
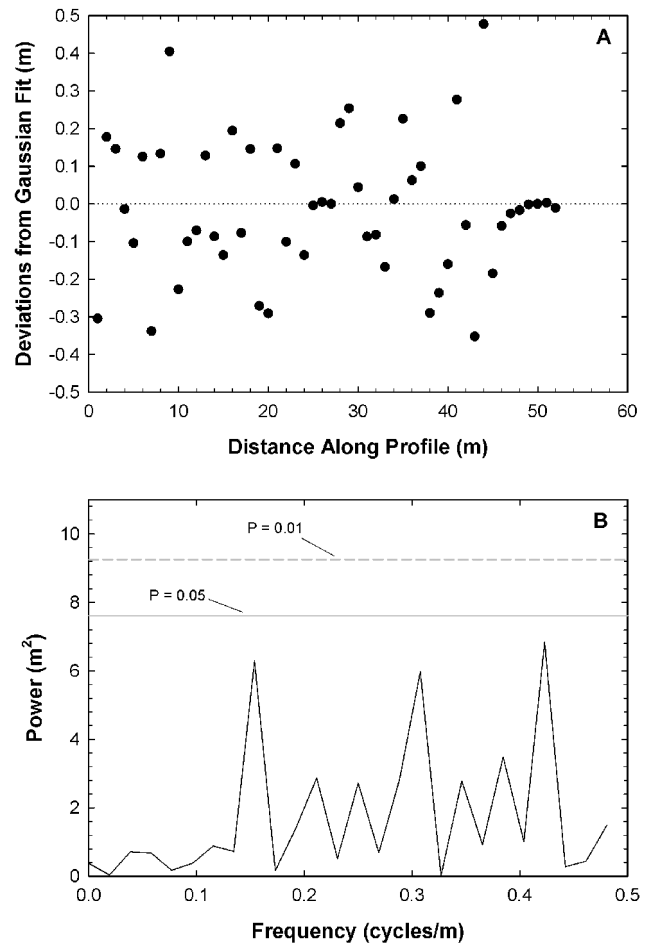
Gaussian shapes approximating a sine wave of the characteristic frequency [*Kean*, 2003]. However, no such characteristic frequencies were found to be present at Ang Nyay (Figure 5b) or at any other sites in this study. This suggests that secondary scales of roughness are absent at the Mekong study sites, though this is discussed further below (section 5). Following *Kean and Smith* [2005], z_{oSF} is approximated by

Table 1. Bank Roughness Parameters Employed in This Study[a]

Sample Location	H_{reg} (m)	σ_{reg} (m)	λ_{reg} (m)	C_D	Number of Bank Roughness Elements	z_{osf} (m)
Ang Nyay	2.37	6.55	14.22	1.26	55	3.7×10^{-4}
Ban Hom	1.82	4.14	10.91	1.34	9	1.9×10^{-2}
Friendship Bridge	1.33	2.62	7.99	1.44	18	1.4×10^{-2}
Pakse	3.81	5.1	22.86	1.51	44	1.6×10^{-2}

[a]H_{reg} is the protrusion height of the bank roughness element, σ_{reg} is the streamwise length scale of the bank roughness element, λ_{reg} is the spacing of the bank roughness element, C_D is the drag coefficient, and z_{osf} is the skin friction roughness height. The subscript "reg" refers to the use of the 88th percentile of the distribution of each bank roughness parameter, this value being used to transform the effects of a sequence of irregularly shaped roughness elements into an equivalently rough surface of regularly spaced identical elements [see *Kean and Smith*, 2006b].

taking a tenth of the standard deviation of the residuals, by analogy to the relation $z_o = 0.1D_{84}$ often used for granular surfaces [e.g., *Whiting and Dietrich*, 1990; *Wiberg and Smith*, 1991]. Details of the bank topographic and skin roughness parameters estimated for the Lower Mekong study sites and used in subsequent computations are summarized in Table 1.

3.1.2. Parameterization of the Outer Flow Velocity

[19] In this study two separate approaches for the specification of the outer region flow velocity were employed, depending on data availability. At two study sites (Ang Nyay and Pakse) measurements of flow velocity were available from a campaign of acoustic Doppler current profiling (ADCP) undertaken as part of another study (I. Conlan, The geomorphology of deep pools on the Lower Mekong River: Controls on pool spacing and dimensions and processes of pool maintenance, manuscript in preparation, 2010). However, field data were not available at the Ban Hom or Friendship Bridge study sites, so Environmental Impact Assessment Centre of Finland (EIA) 3-D hydrodynamic model simulations, again available from a separate prior study [*Koponen et al.*, 2008], were employed instead. Importantly, in both cases estimates of the outer region flow velocity were obtained for a range of flow discharges, allowing τ_{sf} in equation (1) to be related to flow discharge (see section 4.1). In turn, this enables time series of bank erosion rates to be computed using the multidecadal historical flow discharge records that are available at gauging stations located close to the study sites.

[20] Acoustic Doppler current profiler (ADCP) measurements were obtained using a 600 kHz Workhorse Rio Grande ADCP manufactured by RD Instruments mounted approximately 0.35 m below the water surface on a stainless steel frame attached to the side of a survey vessel. Single ensembles were recorded at a ping rate of 1–3 s, depending on flow and depth conditions encountered in each survey. The horizontal position of the boat at each ping was recorded using a Trimble SPS550 Differential GPS at a rate of 2 Hz. Real-time differential corrections were received from the subscription-based Omnistar XP satellite signal, giving submeter position accuracy. Between three and six crossings were made at each cross section during each survey period.

[21] At Ang Nyay, 10 separate surveys at discharges ranging between 1070 m³/s and 13,940 m³/s were undertaken between the end of the dry seasons in May 2006 and April 2007. This range represents the mean annual hydrograph for the nearby Vientiane gauge well, while the maximum discharge recorded in the field surveys is also close to the mean annual peak discharge (1913–2006) of 16,750 m³/s at Vientiane. At Pakse, 11 separate survey missions were undertaken between May 2006 and March 2007 encompassing 17 separate flow discharges ranging from 1930 m³/s and 28,090 m³/s. These flows again bracket the mean annual hydrograph very well, but the largest flow falls below the mean annual peak discharge (37,700 m³/s; 1960–2003) for the Pakse gauge.

[22] To determine the outer region flow velocities, ADCP data were used to quantify transverse variations in depth-averaged flow velocity via nonlinear regression (Figure 6). *Kean and Smith* [2006a] note that the outer region flow velocity must lie at a point (termed the critical distance, z_{crit}) beyond the region of the flow affected by wakes shed by bank roughness elements. However, no observations on the

lateral extent of the wake zone were made during the ADCP surveys. In this study z_{crit} was, therefore, defined as being equal to three times the bank height (H_b), which is assumed to be at a location sufficiently distant from the bank to be safely outside the zone affected by wakes, while not being so distant that the local shear stresses are influenced unduly by transverse variations in channel depth. Note that, because the bank roughness parameters are derived from bank profiles that extend along the study reach, all available ADCP data (i.e., from each cross section and from the multiple traverses at each cross section) were employed in the regressions, thereby accounting for within-reach variability in flow hydraulics. The regression equations were then used to estimate the depth-averaged outer region flow velocity (u_{out}) for the specified value of z_{crit}.

[23] Values of u_{out} and z_{crit} derived in this way and employed in subsequent computations are listed in Table 2. Note that in some cases (e.g., Figures 6a and 6b; see bold text in Table 2 for full list) no clear transverse velocity profile was evident and, in these instances, the outer region flow velocity was estimated simply by averaging all ADCP velocity returns within ±1 m of the z_{crit} location. These instances, particularly at Pakse, correspond to relatively low flows (<4200 and 6600 m³/s for Ang Nyay and Pakse, respectively), and it is likely that flow diversion around midchannel bars and/or islands upstream is responsible for the lack of a well developed transverse flow structure. However, it is later shown (Table 4) that, at Pakse, affected flows are below the threshold for the onset of bank erosion, so any errors introduced do not affect predictions of bank erosion at this location.

[24] At the Ban Hom and Friendship Bridge study sites the EIA 3-D hydrodynamic model was used to simulate the outer region flow velocities across a wide range (5000–15,000 m³/s) of flow discharges. The EIA 3-D model can be classified as a three-dimensional baroclinic multilayer model [*Simons*, 1980; *Virtanen et al.*, 1986; *Koponen et al.*, 1992] and is based on solving simplified Navier Stokes equations on a rectangular model grid. Model simulations (Figure 7) were undertaken using a 50 m horizontal resolution computational mesh that had 10 vertical layers, of which the 9 uppermost layers were 1 m thick and the tenth varied according to the water depth. Both the vertical and horizontal velocities were simulated at the two above mentioned study sites. Vertical velocities are obtained as averages over each grid cell from the continuity equation, so the actual vertical velocities may be significantly higher than the averaged ones.

[25] Outer region flow velocities were estimated using simulated flow velocity data extracted from a 3 × 3 matrix of grid cells surrounding the precise location of the study site. This matrix comprised three grid cells at locations downstream, at, and upstream of the study site, with a further three grid cells extending to a distance of 150 m away from the bank at each of these locations. To provide a representative transverse profile of simulated flow velocity the three estimates of flow velocity within each of the cells in each of the three streamwise-aligned rows were initially averaged. Because the velocity components are calculated in the center of the grid cells (i.e., at distances of 25 m, 75 m and 125 m from the bank), the outer region flow velocity at $z_{crit} = 3H_b$ was then estimated by interpolation (see Table 2 for outer region flow velocities).
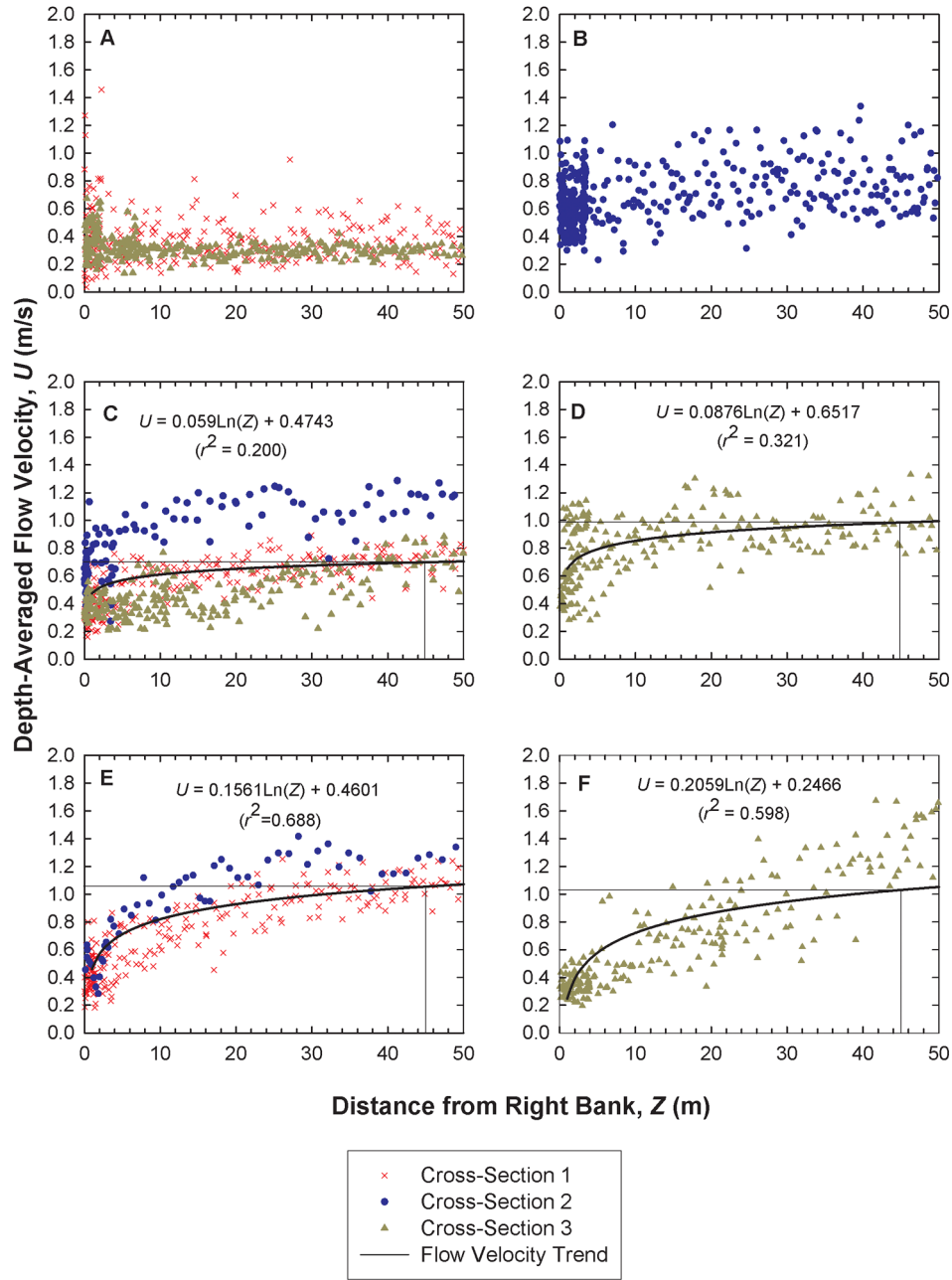
Figure 6. Transverse profiles of depth-averaged flow velocities acquired via acoustic Doppler current profiler (ADCP) measurements at the Pakse study site, for a range of flow discharges (Q). The symbols indicate individual ADCP measurements, whereas the solid lines indicate the fitted trends (regression relationships shown) through these data. The position of the outer flow region (z_{crit}, indicated by the thin vertical line) is equated to $z = 45.0$ m, which is equal to three times the bank height at Pakse. The outer region flow velocity (thin horizontal line) is then estimated based by substituting the value of z_{crit} into the fitted transverse flow velocity profile functions. (a) Flow velocity profile for $Q = 2220$ m³/s; (b) flow velocity profile for $Q = 6590$ m³/s; (c) flow velocity profile for $Q = 11,420$ m³/s; (d) flow velocity profile for $Q = 15,130$ m³/s; (e) flow velocity profile for $Q = 21,560$ m³/s; and (f) flow velocity profile for $Q = 28,090$ m³/s. Note that cross sections 1, 2, and 3 are spaced at 700 m intervals (approximately 0.4 channel widths at this study site).

3.2. Riverbank Erodibility Parameters (τ_c and k)

[26] Estimating the critical shear stress for the fine-grained, cohesive, materials that are the subject of this study is a challenging problem. Unlike granular sediments, the entrainment threshold depends not only on the weight of the grain but additional factors that are difficult to parameterize, including clay and organic content, as well as grain

Table 2. Outer Flow Region Velocities at Specified Distance From the Bank for a Range of Flow Discharge Values at Study Sites Used in This Study[a]

Site	Q (m³/s)	u_{out} (m/s)	z_{crit} (m)
Ang Nyay	1070	1.00	36.0
	1350	1.08	36.0
	2270	**1.25**	**36.0**
	3240	0.95	36.0
	4190	**0.93**	**36.0**
	5420	1.29	36.0
	6360	1.63	36.0
	8860	1.24	36.0
	9070	1.30	36.0
	13940	1.25	36.0
Ban Hom	5000	0.79	42.0
	10000	0.89	42.0
	15000	0.99	42.0
Friendship Bridge	5000	0.55	40.0
	10000	0.74	40.0
	15000	0.84	40.0
Pakse	**1930**	**0.28**	**45.0**
	2220	**0.46**	**45.0**
	2280	**0.40**	**45.0**
	4800	**0.51**	**45.0**
	5430	**0.57**	**45.0**
	6590	**0.69**	**45.0**
	11420	0.92	45.0
	15130	1.06	45.0
	15530	0.92	45.0
	20700	1.30	45.0
	21110	1.17	45.0
	21560	1.11	45.0
	22210	1.20	45.0
	25970	1.25	45.0
	27050	1.15	45.0
	27210	1.31	45.0
	28090	1.29	45.0

[a]Outer flow region velocities, u_{out}; distance from the bank, z_{crit}; and flow discharge values, Q. The outer region flow velocities at the Ang Nyay and Pakse study sites are estimated from ADCP measurements, whereas the outer region flow velocities at Ban Hom and Friendship Bridge are derived from hydrodynamic modeling. Bold text indicates data points at Ang Nyay and Pakse for which no clear transverse velocity gradient was identified from the ADCP data (see section 3.1.2 for details).

mineralogy and the chemical composition of interstitial fluids [*Arulanandan et al.*, 1980; *Grissinger*, 1982]. Thus methods of predicting the erodibility of cohesive bank materials remain poor [*Rinaldi and Darby*, 2007].

[27] An alternative to prediction is to deploy jet testing devices [e.g., *Hanson*, 1990; *Hanson and Simon*, 2001; *Clark and Wynn*, 2007; *Thoman and Niezgoda*, 2008] to obtain direct measurements of bank erodibility in situ. These devices operate by directing jets of water with known, progressively increasing, hydraulic properties at the bank materials. Eventually the jet becomes sufficiently strong to initiate erosion, the depth of the resulting scour hole being measured periodically with a mechanical point gauge, until an equilibrium scour depth is attained. The measured erosion rate, scour depth and known hydraulic properties are then used to back-calculate the erodibility parameters. The development and use of jet testers of this type represents an important advance in that both (τ_c and k) erodibility parameters are directly measured in situ, while the small scale of the impinging jet means that scale problems associated with the larger sampling footprint of devices such as portable flumes [*Tolhurst et al.*, 2000; *Aberle et al.*, 2006; *Widdows et al.*, 2007] are eliminated. However, the large size and weight of the equipment, and the need for peripherals such as a pump and hoses, make the deployment of established jet testing devices unwieldy, particularly in remote locations. In addition, on resistant surfaces, errors involved in mechanically inserting the point gauge into the base of the scour hole can be similar in magnitude to the scour depth itself, while erodible materials generate scour depths that can exceed the extent of the gauge. Moreover, it is recognized that natural cohesive materials are highly variable [e.g., *Arulanandan et al.*, 1980; *Grissinger*, 1982; *Thorne*, 1982; *Samadi et al.*, 2009], which necessitates repeat sampling. Because individual tests are time consuming (~0.5 h), it is difficult to obtain the replicate samples needed to characterize the inherent variability of fine-grained bank materials.

[28] Alternative instruments such as the cohesive strength meter (CSM) [*Tolhurst et al.*, 1999], which have been
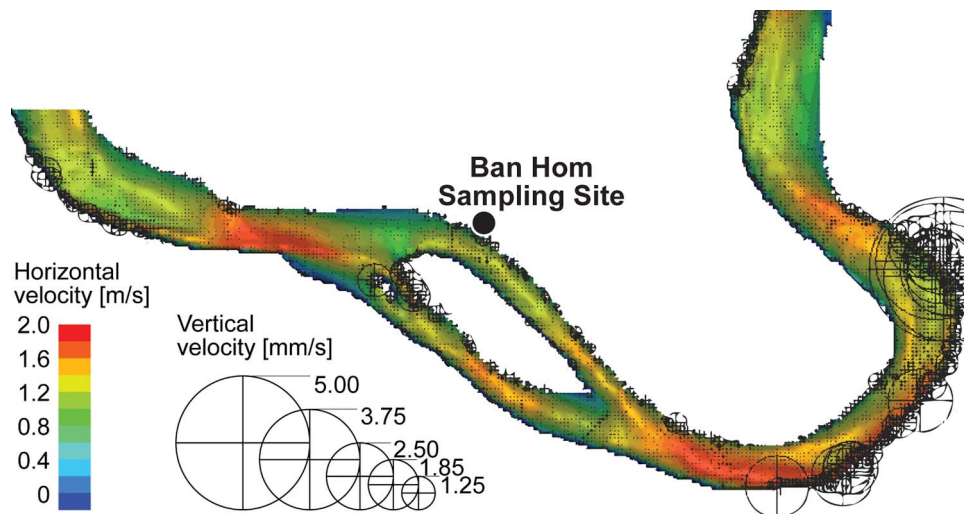

Figure 7. Example of simulated horizontal (colors) and vertical (crosses and circles) flow velocities from the EIA 3-D model for a reach of the Lower Mekong River encompassing the Ban Hom (location shown on the diagram) study site for a flow discharge of 12,000 m³/s.
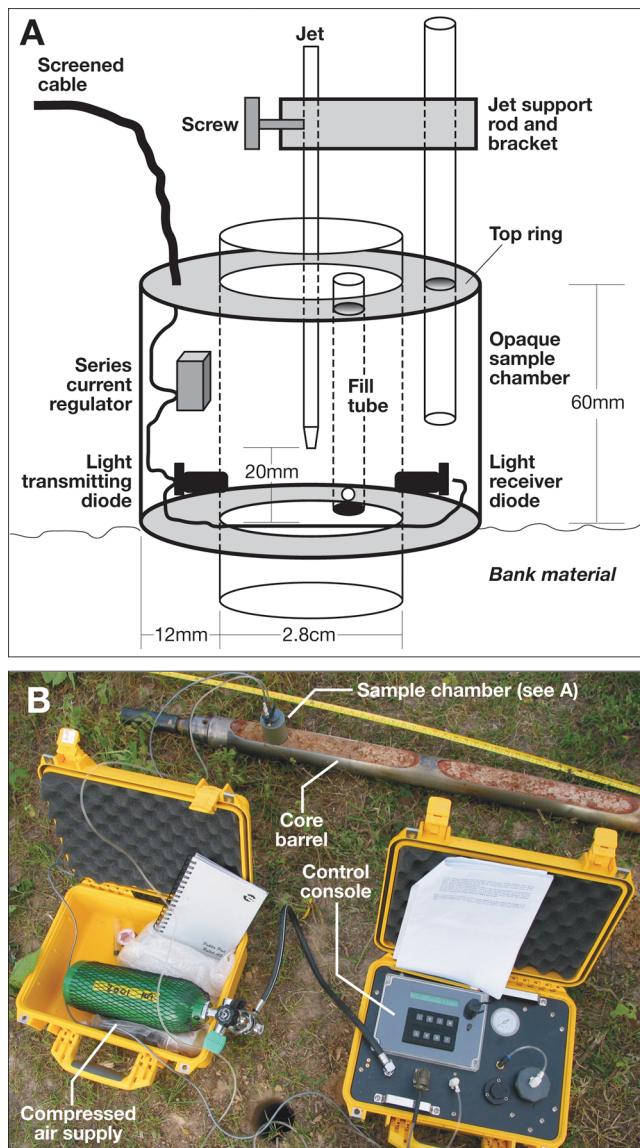
Figure 8. Diagram illustrating the cohesive strength meter apparatus employed in this study. (a) Detailed view of the sampling chamber [after *Tolhurst et al.*, 1999]. (b) Method of deploying the sampling chamber into bank toe sediments extracted using the core barrel.

widely employed in studies of intertidal flat sediments [*Paterson*, 1989; *Tolhurst et al.*, 1999; *Tolhurst et al.*, 2000], but have not been used yet for studies of fine-grained riverbank erosion, appear to offer some advantages over conventional jet testing devices. The CSM operates in similar fashion, firing submerged jets of increasing intensity at the target surface. However, the CSM detects the onset of erosion by monitoring optical transmission within an opaque test chamber that houses the brass jet nozzle (1 mm internal diameter) and infrared transmitter and receiver diodes (Figure 8a). An onboard data logger records the jet pressure and optical transmission values at and after each pulse. The moment of erosion is detected via drops in optical transmission induced by the suspension of eroded sediment, with the jet properties

at that threshold used to define the critical stress. The test chamber consists of two concentrically located plastic cylinders, the outer one (external diameter 5.6 cm, internal diameter 2.8 cm) encasing the diodes and filling tubes (Figure 8a), and the inner one (internal diameter 2.8 cm, external diameter 3.0 cm), enclosing a sediment sampling footprint of 6.6 cm^2 [*Tolhurst et al.*, 1999]. Before a test, the chamber is inserted carefully into the sediment by pushing it flush to the surface prior to being gently (so as to avoid disturbing the sediment surface) filled with water via a syringe directed into a tube set within the test chamber wall. Tests are both automated and rapid (typically less than 3 min in the configurations employed in this study) so large numbers of samples can readily be obtained, while its relatively small size (Figure 8b) and weight (13 kg) enable operatives to deploy the CSM in remote locations and on steep riverbanks that would otherwise be difficult to access.

[29] In this study the CSM was used to determine the erodibility of bank toe materials. A focus on bank toe material is appropriate because long-term rates of bank erosion are known to be controlled by toe erosion [*Thorne*, 1982; *Rinaldi and Darby*, 2007]. Note that the bank "toe" in this context refers to the lower part of the bank profile, that is accordant with the location of the bank roughness profiles described previously. Where possible, samples were accessed by climbing down to the exposed toe and inserting the CSM test chamber directly into the bank face. More commonly, the bank toe was not accessible. In these cases bank toe materials were extracted by means of an open core barrel driven by means of a percussion corer into a vertical borehole located on the floodplain surface close to the bank edge. After removing the core from the borehole, the outer disturbed portion of the core was cleaned using a sharp knife. The CSM test chamber was then inserted directly into the materials exposed in the open barrel (Figure 8b).

[30] At the Pakse study site bank toe materials were sampled both by direct access and by coring. A simple *t* test indicates that there is no significant difference (at 99.9% confidence) between the two types of samples, providing some degree of confidence that the sampling method does not adversely affect the results. The CSM enables users to select from an array of test sequences that control test parameters such as the pulse duration, optical transmission logging parameters, initial and final pulse strength and pulse increments. In all cases reported here the test sequence used an initial pulse pressure of 3.45 kPa, incremented at 3.45 kPa intervals to a maximum value of 137.90 kPa. Pulse duration was 1 s and optical transmission values were logged for 3 s at 0.1 s intervals after each pulse, with the jet nozzle deployed at a height of 2.0 cm above the sediment surface.

[31] Post processing involved plotting optical transmission, averaged in the period between 0.2 and 1.2 s after each pulse [*Black and Tolhurst*, 2000], versus jet pressure for each of the individual tests undertaken at each site (Figure 9). Outliers were inspected carefully to evaluate whether blunders had been made during testing and, where necessary, such few instances (not shown here) were removed from further analysis. It is important to note that outliers were only removed if there was clear evidence that human error (usually associated with the inadvertent presence of sediment on the optical transmission diodes) had been made. Thus, while Tests 17, 18 and 25 at Ban Hom (Figure 9b), and Test 36 at
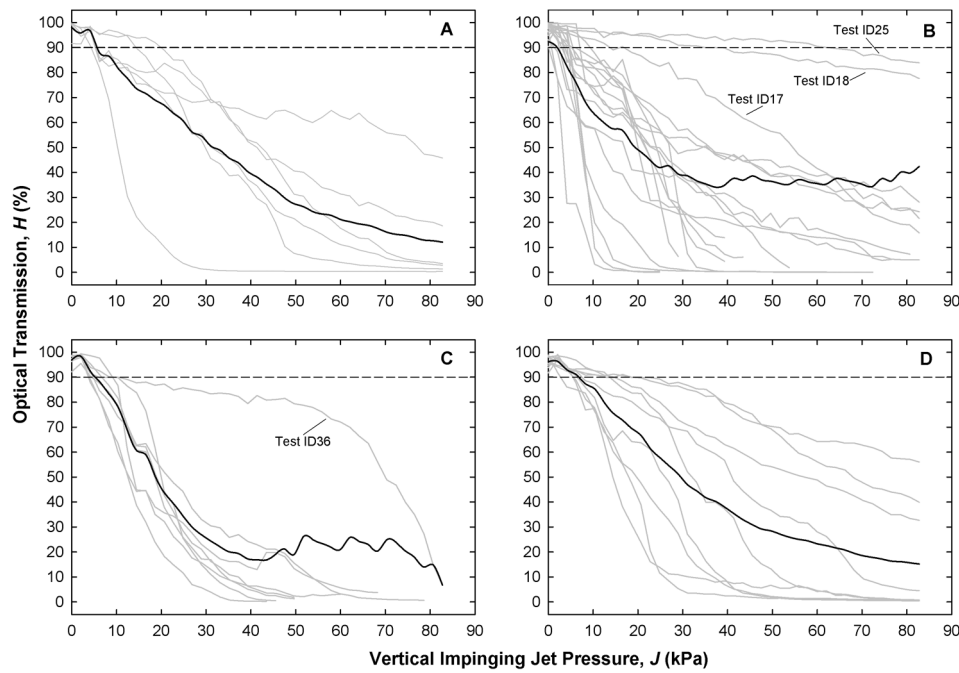
Figure 9. Curves of optical transmission (H) (measured in percent) versus vertical jet pressure (J) (measured in kilopascals) for the CSM test results obtained at the (a) Ang Nyay, (b) Ban Hom, (c) Friendship Bridge, and (d) Pakse study sites. Individual tests results are illustrated by the thin gray curves; the solid black curves indicate the mean of each ensemble. The horizontal dashed lines indicate the critical optimal transmission value (90%) used to define the onset of erosion.

Friendship Bridge (Figure 9c), all appear to follow different trajectories relative to other tests in their respective ensembles, no evidence of any sampling errors was noted and therefore all were included in subsequent analysis. The inclusion of Test 36 at Friendship Bridge has no significant effect on the derived bank erodibility statistics, because divergence from the other tests in the ensemble only occurs after the threshold for onset of erosion has been attained.

[32] Regarding this threshold condition, a standard criterion for the vertical jet pressure at the onset of erosion was defined as the point at which the optical transmission drops below 90% of its initial value [*Black and Tolhurst*, 2000]. The vertical jet pressure at the onset of erosion (J, in kPa) is calibrated to an equivalent horizontal critical shear stress (i.e., τ_c) using [*Tolhurst et al.*, 1999],

$$\tau_c = 66.6734(1 - \exp(-J/310.09433)) \\ - 195.27552(1 - \exp(-J/1622.56738)), \quad (18)$$

with equation (18) being developed by subjecting unimodal quartz particles to both (1) CSM tests and (2) laboratory

flume investigations to calculate the critical shear stress (see *Tolhurst et al.* [1999] for details). Unlike conventional jet testing devices, which provide estimates of both τ_c and k, the CSM provides only the critical shear stress. Advantage is therefore taken of the strong inverse relationship between τ_c and k [*Arulanandan et al.*, 1980; *Hanson and Simon*, 2001], with k being calculated using an empirical relationship ($n = 83$; $r^2 = 0.64$) derived from jet testing data obtained by *Hanson and Simon* [2001] (modified here for the units employed in this study):

$$k = 2.0 \times 10^{-7} \left(\tau_c^{-0.5} \right). \quad (19)$$

The τ_c and k values so obtained are listed in Table 3.

4. Results

4.1. Applying the Model

[33] The preceding analyses were used to provide estimates of bank erosion rate as follows.

[34] 1. The bank roughness (Table 1) and outer region flow velocity data (Table 2) were initially employed to calculate

Table 3. Erodibility Parameters of Bank Toe Materials Investigated in This Study

Sample Location	Bank Toe Material	Sampling Method	τ_c[a] (Pa)	k (m^2 s/kg)	Number of Samples
Ang Nyay	silt ($D_{50} = 19 \ \mu$m)	core	0.83 ± 0.57	2.20×10^{-7}	6
Ban Hom	silt ($D_{50} = 36 \ \mu$m)	exposed toe material	0.84 ± 1.16	2.18×10^{-7}	19
Friendship Bridge	very fine sand ($D_{50} = 82 \ \mu$m)	exposed toe material	0.56 ± 0.20	2.67×10^{-7}	8
Pakse	fine silt ($D_{50} = 9 \ \mu$m)	exposed toe material	0.88 ± 0.47	2.13×10^{-7}	9

[a]Critical shear stress (τ_c) values listed here are the mean ±1 standard deviation.
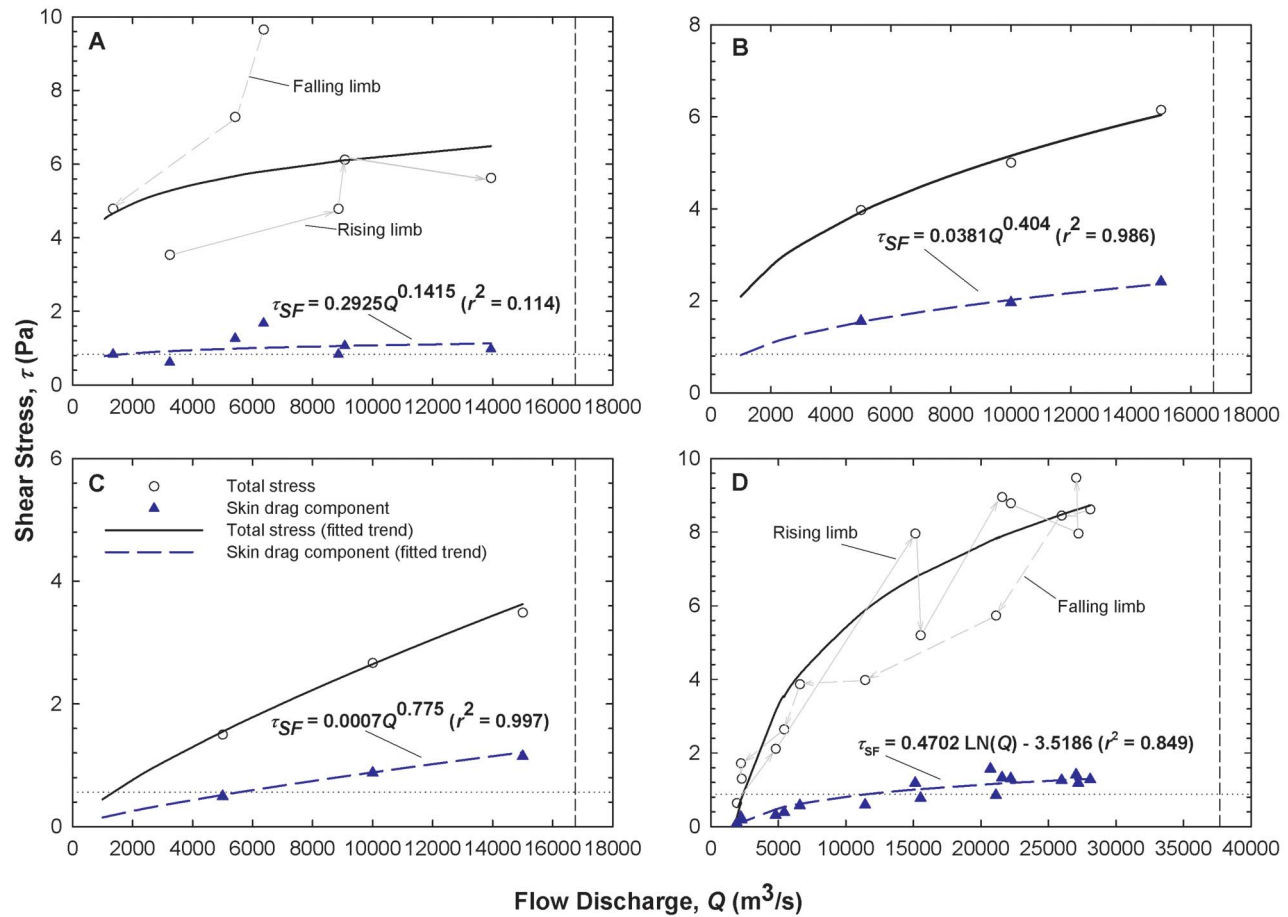
Figure 10. Simulated bank boundary shear stresses as a function of flow discharge for study sites at (a) Ang Nyay, (b) Ban Hom, (c) Friendship Bridge, and (d) Pakse. The horizontal lines indicate the mean critical shear stress values estimated from CSM measurements in this study. Vertical lines indicate the mean peak discharge observed at the gauging stations at Vientiane (for the Ang Nyay, Ban Hom, and Friendship Bridge study sites) and Pakse (for the Pakse study site). The regression relationships linking the total stress (solid lines) and skin drag component (dashed lines) of bank boundary shear stress to the flow discharge at each study site, with the latter being used in the bank erosion modeling, are also shown. At Ang Nyay and Pakse the temporal sequence of sampled flow events across the rising and falling limbs of the flood hydrograph is indicated by the gray arrows (shown for the total bank boundary shear stress only).

the bank boundary shear stress components, using the Kean and Smith model as described above. An Interactive Data Language (IDL) script written by Jason Kean was used for this purpose. Note that the availability of outer region flow velocity data for a range of flow discharges enabled multiple simulations to be undertaken, thereby obtaining total, form and skin drag components of boundary shear stress across a wide range of flow discharges.

[35] 2. The simulated boundary shear stress components obtained in Step 1 were then linked to flow discharge using bivariate regression (Figure 10). In all cases significant (P < 0.001) regression relationships were obtained. A wide range of models (logarithmic, power, etc) were explored, with the selected relationships initially chosen simply on the basis of those that provided the best fit. However, at Pakse the best fit ($r^2 = 0.951$) initially was obtained using a second-order polynomial. This model was rejected on the basis that a decline in applied boundary shear stress at flow discharges

higher than the function's local maximum ($Q \approx 45000$ m^3/s) is physically unrealistic. The favored logarithmic curve (Figure 10d) still provides a very good fit ($r^2 = 0.918$), but ensures that simulated boundary shear stresses monotonically increase with flow discharge. At one study site (Ang Nyay, Figure 10a) there is evidently hysteresis in the relationship between the flow discharge and simulated bank boundary shear stress, this being caused by hysteresis in the relationship between discharge and the outer region flow velocity. The cause and implications of this hysteresis are discussed further below (section 6).

[36] 3. The fitted relationships between bank shear stress and flow discharge were next used to reconstruct daily variations in applied shear stress using mean daily discharge records from the Vientiane and Pakse flow gages. Note that, for the highest flow discharges in the record (25,900 m^3/s in 1966 at Vientiane; 56,000 m^3/s in 1978 at Pakse), the fitted relationships (Figure 10) must be extrapolated beyond the
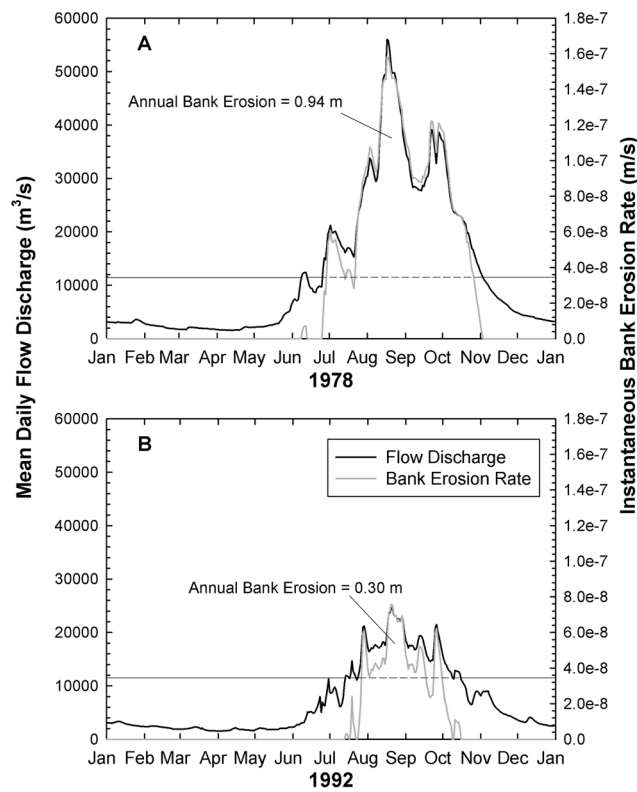
Figure 11. Time series of instantaneous simulated bank erosion rates (gray lines) at the Pakse study site induced by selected annual flood hydrographs (black lines): (a) 1978, a high flow year (the peak discharge of 56,000 m^3/s being the highest on record) that forces the highest annually integrated rate of bank erosion (0.94 m) in the simulation period 1961–2007; and (b) 1992, a low flow year with the corresponding lowest annually integrated rate of bank erosion (0.30 m) during 1961–2007. Note that all the plots are scaled identically and that the mean annual bank erosion rate during 1961–2007 is 0.61 m/yr. The horizontal lines indicate the threshold flow discharge (Q_c = 11,555 m^3/s) for the initiation and cessation of bank erosion, where the solid portion indicates periods when the flow is below the threshold (no erosion) and the dashed portion indicates periods when the flow exceeds the threshold. The volume of runoff contained between the dashed line and the solid curve of the annual hydrograph therefore effectively determines the annual erosion rate.

range of data used to construct them. This procedure is potentially problematic in that the simulated shear stress values within the extrapolated domain induce the highest instantaneous simulated bank erosion rates, but the relatively low duration of these flows must also be recognized. For example, exceedance probabilities of flows within the extrapolated range are less than 3.4% ($Q > 13,940$ m^3/s) at Ang Nyay, and less than 2.1% ($Q > 15,000$ m^3/s) at Ban Hom and Friendship Bridge. However, extrapolated flows have a slightly larger exceedance probability of 7.8% ($Q > 28,090$ m^3/s) at Pakse. Although the gauging stations have records dating from 1913 and 1923, respectively, simulations in this study were initialized either at 1959 (Ang Nyay and Pakse) or 1961 (Ban Hom and Friendship Bridge), to coincide with the availability of data used in the model validation (see section 4.2).

[37] 4. The reconstructed daily shear stress time series were then used in equation (1), together with the values of τ_c and k derived from the CSM measurements (Table 3), to develop time series of simulated instantaneous bank erosion rates at daily time steps. Simulations were repeated for scenarios in which erodibility parameters were set using (1) the mean critical shear stress values (Figure 11 and Table 4) plus (2 and 3) a range of erodibility parameters with limits corresponding to plus or minus one standard deviation about the mean critical stress (Table 4).

[38] Two illustrative examples of model outputs obtained by following the above procedure are shown in Figure 11 for the Pakse study site. It is worth reiterating that, to the best of our knowledge, these simulations represent the first simulations of hydraulic bank erosion that are obtained without recourse to calibration. Furthermore, in addition to the strong physical basis of the model, the availability of the regression relationships linking simulated bank boundary shear stress and flow discharge (Figure 10) provides a means to obtain simple bank erosion rate predictions that are linked directly to the controlling flow discharge regime. In fact, Figure 11 shows that it is the accumulated volume of runoff above the threshold discharge required to initiate bank erosion, $\Sigma(Q - Q_c)$, which is the key hydrological control on bank erosion. For the LMR at Pakse, variations in $\Sigma(Q - Q_c)$ are induced primarily as a result of interannual variability in the magnitude of the annual flood. Thus, during the period 1923–2009 the highest (0.94 m) and lowest (0.30) annual rates of bank erosion occurred in years with the highest (56,000 m^3/s, in 1978) and lowest (24,600 m^3/s, in 1992) peak flow discharges (Figures 11a and 11b). Peak flows are controlled primarily by the intensity of the monsoon (more specifically, the volume of monsoonal rainfall falling in the Mekong catchment), but any simple link between monsoon intensity and bank erosion is masked by the fact

Table 4. Computed Bank Erosion Statistics for the Various Study Sites[a]

Study Site	Simulation Period	Threshold Flow Discharge for Onset of Bank Erosion, Q_c (m^3/s)	Cumulative Simulated Bank Toe Erosion (m)	Mean Annual Rate of Simulated Bank Toe Erosion (m/yr)
Ang Nyay	1961–2007	1590 (0–63,920)	32.6 (0.0–391.6)	0.68 (0.0–8.2)
Ban Hom	1961–2005	2115 (0–18,100)	77.9 (0.1–2020.4)	1.76 (0.0–45.6)
Friendship Bridge	1961–2005	5570 (3150–8260)	32.2 (12.7–78.2)	0.73 (0.3–1.8)
Pakse	1961–2007	11,555 (4250–31,390)	29.3 (0.8–137.7)	0.61 (0.0–2.9)

[a]Values in parentheses indicate the range of values induced by using critical shear stress values of ±1 standard deviation from the mean.

Table 5. Summary of Data Sets Used to Determine Bankline Positions at the Various Study Sites

Study Site	Data Sets Employed	Error	Erosion Epoch Used in Analysis	Cumulative Error
Ang Nyay	1959 aerial imagery	±20.4 m	1959–2000 (41 years)	±35.4 m (±0.86 m/yr)
	Landsat satellite image (1/4/2000)	±15 m		
Ban Hom	1961 Hydrographic Atlas	±1.4 m	1961–1992 (31 years)	±4.0 m (±0.13 m/yr)
	1992 Hydrographic Atlas	±2.6 m	1992–2005 (13.33 years)	±5.1 m (±0.38 m/yr)
	SPOT5 satellite image (28/4/2005)	±2.5 m		
Friendship Bridge	1961 Hydrographic Atlas	±1.4 m	1961–1992 (31 years)	±4.0 m (±0.13 m/yr)
	1992 Hydrographic Atlas	±2.6 m	1992–2005 (13.33 years)	±5.1 m (±0.38 m/yr)
	SPOT5 satellite image (28/4/2005)	±2.5 m		
Pakse	1959 aerial imagery	±4.5 m	1959–2009 (50 years)	±5.0 m (±0.1 m/yr)
	GeoEye satellite image (10/4/2009)	±0.5 m		

that $\Sigma(Q - Q_c)$ depends also on interannual variations in the duration of flows above the threshold. The latter is a complex function of variations in the timing of the onset and cessation of the monsoon, as well as variations in the contribution to summer base flows of glacier and snowmelt from Tibetan source regions. Detailed analysis of the effects of hydro-climatological variability and change on bank erosion is beyond the scope of this paper, but the ability of the new model to obtain a simple, but physically based, link between flow discharge and simulated bank erosion rates means that it is well suited for such investigations. In practice it is necessary to have confidence in the model's predictions, so attention is now turned to evaluating the performance of the new model.

4.2. Model Evaluation

[39] Model predictions were evaluated by comparing simulated bank erosion rates with those estimated by analysis of map data and remotely sensed imagery. In the case of the Ban Hom and Friendship Bridge study sites, observed rates of erosion were determined in a study by *Kummu et al.* [2008]. In summary, *Kummu et al.* [2008] employed three main spatial data sets:

[40] 1. The 1:20,000 scale Hydrographic Atlas of 1961 [*Mekong River Commission*, 1961], which is based on field surveys and aerial photographs recorded between 1959 and 1961. Images from the atlas were scanned and geo-referenced to an average root-mean-square error (RMSE) of ±1.4 m (see *Kummu et al.* [2008] for full details), prior to the bank-lines being digitized and converted into a shape file for use in GIS analysis.

[41] 2. The 1:20,000 scale Hydrographic Atlas of 1992 [*Mekong River Commission*, 1992], which is based on aerial photos acquired in 1991/1992. This atlas is already available in digital format, so scanning was not necessary, but the images were in this case geo-referenced to an average RMSE of ±2.6 m (see *Kummu et al.* [2008] for full details).

[42] 3. A rectified SPOT5 satellite image acquired on 28 April 2005 and with a resolution of 2.5 m was used to map the bank locations in 2005 [*Kummu et al.*, 2008].

[43] The 1961 Hydrographic Atlas provides aerial photos of the entire Lower Mekong River and the original 1959 aerial photos used in the derivation of the Atlas were therefore employed at the Ang Nyay and Pakse study sites. The 1959 images were supplemented with more recent ones. At Pakse a rectified 0.5 m resolution GeoEye satellite image, acquired on 10 April 2009, was used. Control points visible on the 2009 satellite image and on the 1959 aerial images were used

to geo-reference the 1959 images to the 2009 image (RMSE equals ±4.5 m), using a total of 12 control points. At Ang Nyay recent high-resolution imagery was not available, so a 15 m resolution Landsat image, acquired on 1 April 2000, was used instead. The 1959 images were georeferenced to the Landsat image, in this case using a total of 7 control points (RMSE equals ±20.4 m). The bankline positions on each image were then digitized and the Digital Shoreline Analysis System (DSAS) of *Thieler et al.* [2009] was used to cast transects across the banklines and thus determine the amount of bank top retreat during the measurement interval at the two sites. These various data sets provide a total of 6 epochs of observed bankline shift, with identified errors, across the four study sites (Table 5).

[44] A comparison of simulated versus observed data is shown in Figure 12. It is emphasized that observed rates of bank erosion strictly correspond to shifts in the position of the bank top identified from the satellite images/aerial photographs, whereas model simulations correspond to rates of bank toe erosion. The assumption that long-term rates of bank retreat are forced by rates of bank toe erosion (see section 6) is, therefore, pertinent. Note that predictive uncertainty (associated with scenarios 2 and 3 outlined in section 4.1 (step 4), and illustrated by the horizontal error bars on the plot) are large, reflecting the high natural variability of bank material erodibility (Table 3). Consequently, the predictive uncertainty bands overlap the line of perfect agreement for four of the six data points presented on Figure 12 (the exceptions being the 1959–1992 and 1992–2005 epochs at Friendship Bridge). The measurement errors are smaller than the predictive uncertainty bands (measurement errors range from 0.10 to 0.86 m/yr (see Table 5) and are illustrated by the vertical error bars on the plot), so only two data points to overlap the line of perfect agreement. That is, four to five of the six available data points plot sufficiently close to the line of perfect agreement to intersect it, within the bounds of the (albeit large) uncertainty inherent in the analysis.

[45] A linear regression equation of the form $\varepsilon_{obs} = c + m \, \varepsilon_{pred}$ was used to compare observed and simulated erosion rates quantitatively. Note that due to the low number of data points, the regression was undertaken using a non-parametric [*Theil*, 1950; *Sen*, 1968] regression estimator. The values of the gradient ($m = 0.303$) and intercept ($c = 0.374$) obtained via Theil-Sen regression indicate the general tendency of the model to overpredict (RMSE equals ±0.53 m/yr), though the low value of the coefficient of
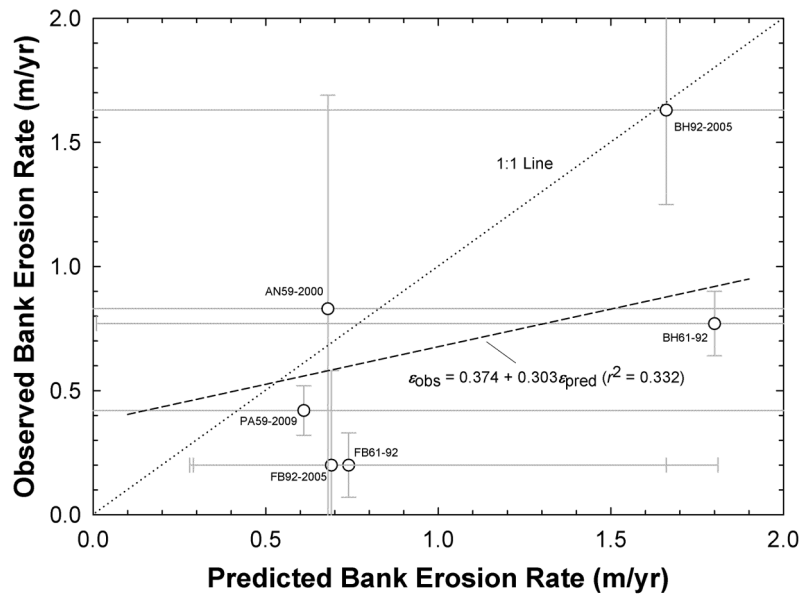
Figure 12. Comparison of predicted and observed bank erosion rates at the study sites on the Lower Mekong River. The vertical error bars indicate image analysis errors (see Table 5 for details), whereas the horizontal error bars reflect prediction uncertainty associated with a ±1 standard deviation range in the critical shear stress values employed in the analysis. Data points are labeled as follows: AN59-2000 for the Ang Nyay study site; PA59-2009 for the Pakse study site; FB61-92 and FB92-2005 denote the Friendship Bridge study site for the 1961–1992 and 1992–2005 epochs, respectively, and; BH61-92 and BH92-2005 denote the Ban Hom study site for the 1961–1992 and 1992–2005 epochs, respectively. The line of perfect agreement (dotted) and the Theil-Sen regression line (dashed) through the data points are also shown.

determination of the regression ($r^2 = 0.332$) highlights the considerable scatter in the limited data set employed here.

[46] It is stressed that the number of data points (6) employed in this analysis is clearly less than would be ideal for a comprehensive analysis of model performance. However, the logistical difficulties involved in collecting the data necessary to parameterize, and particularly to validate, the model should be recognized. A key limiting factor concerns the lack of available satellite imagery or aerial photographs of sufficiently high resolution and at frequent temporal intervals. As such the validation presented in Figure 12 provides only a tentative indication of model performance and further work is required to assess model capability across a wider range of river contexts than has been possible herein. As such, it is appropriate to consider the nature of likely model error from first principles (section 5) and as informed by model sensitivity analysis.

4.3. Sensitivity Analysis

[47] To investigate the relative importance of the different factors controlling simulated rates of bank erosion, and to better understand how predictive uncertainties might be generated by errors in the parameterization of these factors, a series of model sensitivity analyses were undertaken. In these sensitivity analyses the roughness, flow and bank erodibility input data for the Pakse study site (see Tables 1–3) were used as baseline parameters. Simulations were undertaken using the mean annual hydrograph as determined from hydrological records at the Pakse gauge for the period 1923–

2007, 1923 being the earliest date for which data are available. With these input parameters a mean annual rate of hydraulic erosion of 0.60 m/yr is obtained. Note that this differs very slightly from the mean annual rate of erosion (0.61 m/yr) simulated previously, the difference being caused by the use of a mean annual hydrograph for the monitoring period 1961–2007 in the prior simulations. Individual sensitivity tests were undertaken for the six model input parameters that represent different aspects of the bank roughness (H, σ, λ, z_{oSF}), outer region flow (u_{out}) and bank material erodibility (τ_c). In each case sensitivity tests were undertaken by systematically perturbing these input parameters across an arbitrarily selected range of ±25% relative to its baseline state, while holding all the other parameters at their baseline values.

[48] Results of the sensitivity analyses are illustrated in Figure 13. It is immediately clear that model response to changes in input parameters is highly sensitive. Variations in all six input parameters induce relative increases in simulated bank erosion rates (ranging from a factor of about 0.8 (for z_{oSF}) to a factor of 3.6 for u_{out}) that are much greater than the ±25% perturbation in each input parameter. It should also be noted that the nonlinear response of bank erosion rate to perturbations in many of the input parameters suggests that the extent to which model response is sensitive is likely to be site specific. For example, model response to the bank roughness parameters is more sensitive on smoother banks (low H, σ and z_{oSF} values), whereas model sensitivity is dampened on rougher banks. In the extreme case of banks that
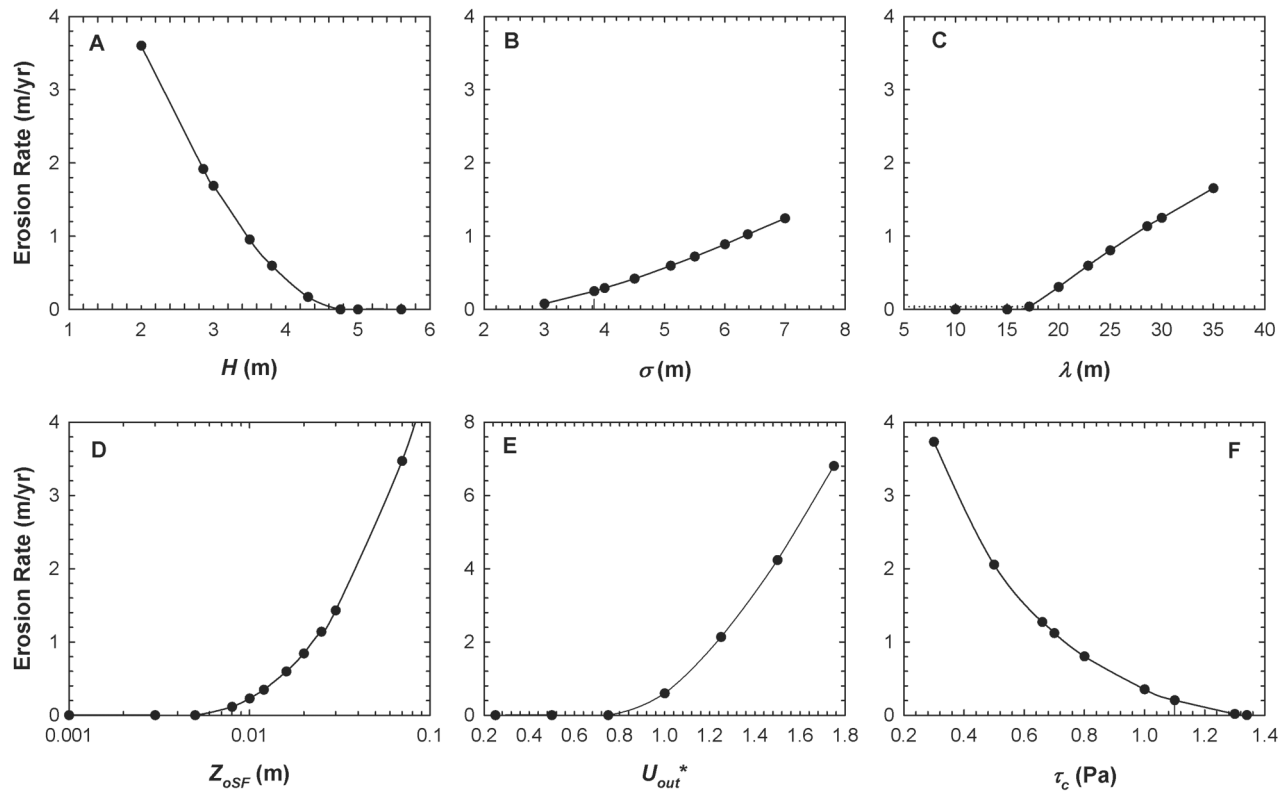
Figure 13. Sensitivity of simulated annual rates of bank erosion to variations in model input data parameters: (a) bump protrusion height (H, in meters); (b) Bump length (σ, in meters); (c) bump spacing (λ, in meters); (d) skin roughness height (Z_{oSF}, in meters); (e) nondimensional outer region flow velocity (u_{out}^*, in meters per second); and (f) critical shear stress (τ_c, in pascals). Annual erosion rates are calculated based on the mean annual hydrograph (1923–2005) for Pakse. Note the change in the vertical scale in Figure 13e.

are so rough that the applied skin drag component of fluid stress is insufficient to surpass the critical shear stress, simulated erosion rates and hence sensitivity of erosion rate to variations in input parameters, both fall to zero. This observation emphasizes the importance of accurate estimation of all the input parameters employed in the model, but with particular emphasis on characterizing the outer region flow and the macro-scale bank roughness. The significance of this latter point is discussed further below (section 5).

4.4. Influence of Form Roughness on Boundary Shear Stress and Bank Erosion

[49] It is noteworthy that the bank shear stress values obtained are rather small (<10 Pa), even at flow discharges that exceed 25,000 m³/s. This result is not unreasonable given the low channel gradients encountered on this large river. Moreover, the significance of the form drag component in the shear stress partitioning is also evident, this component accounting for between 61% (Ban Hom) and 85% (Pakse) of the total stress imparted on the banks. The large form drag component has the effect of reducing the skin drag component to values similar to the estimated critical shear stresses, the latter being indicated by the horizontal dashed lines in Figure 10. Assuming that the CSM data provide a reliable representation of these erosion

thresholds, the large magnitude of the form drag components of boundary shear stress therefore suggests that approaches which fail to account for the form drag (i.e., which assume $\tau_d = 0$) would result in gross overestimates of bank erosion.

[50] This is illustrated by comparing annual bank erosion rates (during 1961–2007) simulated at each of the Ang Nyay (0.68 m/yr versus 30.8 m/yr), Ban Hom (1.76 m/yr versus 12.46 m/yr), Friendship Bridge (0.73 m/yr versus 6.62 m/yr) and Pakse (0.61 m/yr versus 21.0 m/yr) study sites for scenarios with (first quoted figures) and without (second quoted figures) the form drag component (i.e., using the total drag and skin drag curves in Figure 10, respectively). Thus simulated rates of bank erosion as obtained assuming zero bank roughness are greater than the rates obtained when including the bank form drag by factors that vary between about 7.1 (Ban Hom) and 45.3 (Ang Nyay). As such, the presence of high bank form roughness, induced by the presence of irregular bank topography, can be viewed as an important factor that self-limits the rate of bank erosion.

5. Discussion: Potential Sources of Model Error

[51] Assuming that the data presented in Figure 12 reflect a true tendency for the model to overpredict bank erosion rates, it follows that the source of error must either lie in
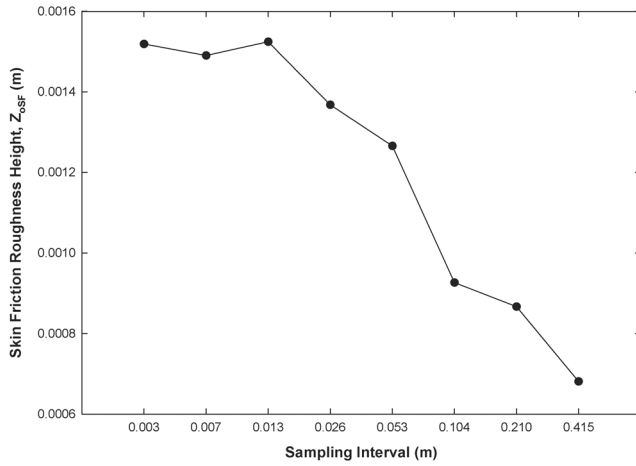
Figure 14. Influence of the spatial resolution of bank topographic profiles on estimates of skin friction roughness height (z_{oSF}) as derived from a 2008 laser scan survey of a riverbank on the Cecina River, Italy.

overestimation of computed values of τ_{sf}, or underestimation of τ_c (and therefore k), or both. In fact, systematic under-estimation of τ_c is consistent with recent work [*Vardy et al.*, 2007] which has suggested that the CSM calibration relationship (equation 18) should be expressed in terms of the jet pressure exerted on the sediment surface, not the jet pressure at the nozzle exit as in equation 18, with formulations based on the latter underestimating the true critical stress [*Vardy et al.*, 2007]. Unfortunately, revised calibrations for the CSM model (Mark IV) used in this study are not yet available.

[52] Inaccurate estimation of τ_{sf} could be induced via inaccurate parameterization of any or all of the outer region flow velocity (u_{out}), bank macro-scale roughness (H_{reg}, σ_{reg}, λ_{reg}) or skin friction roughness height (z_{oSF}) parameters. The sensitivity analyses (Figure 13) indicate that small errors in u_{out} can have a large affect on τ_{sf} and thus bank erosion rates, but misparameterization of u_{out} is unlikely responsible for overprediction of bank erosion in this study. This is because Figure 6 shows that, if anything, the value of u_{out} is underestimated, which would lead to underestimation (not overestimation) of τ_{sf}. Significant error in the values of H_{reg}, σ_{reg}, λ_{reg} also appears unlikely given the high quality of the Gaussian fits achieved with the bank topographic data in this study.

[53] An alternative explanation for possible overestimation of τ_{sf} is that, although the 0.50 m sampling interval used to survey bank topographic profiles may be sufficient to capture adequately the macro-scale bank roughness, the sampling interval may be too coarse to determine z_{oSF} accurately. Moreover, in some rivers, bank roughness is characterized by a hierarchy of different sized topographic features, with the total stress being partitioned between the skin-friction grain roughness, as well as the form roughness on meso- and macro-scale bank form roughness elements (e.g., Rio Puerco bank roughness discussed by *Kean and Smith* [2006b]). The coarse sampling interval employed in this study opens the possibility of there being unresolved form

drag producing secondary roughness at the meso-scale, which would reduce τ_{sf} and predicted erosion rates.

[54] The extent to which unresolved micro- and meso-scale roughness may be significant on the banks of the Mekong remains unknown, but to demonstrate how the coarse sampling interval employed in this study may affect the estimation of z_{oSF} a series (5, distributed at equidistant vertical intervals) of longitudinal bank roughness profiles were extracted from a mean 3 mm resolution TIN model constructed from a high-resolution (mean point density ~57,000 pts/m^2) topographic survey, the latter being acquired through terrestrial laser scanning (TLS). The scan was undertaken in September 2008 at a riverbank on the Cecina River in Italy (see *Luppi et al.* [2009] for a description of this study site). Bank roughness profiles extracted from the TIN were systematically decimated so as to simulate the effects of varying sampling interval on the resulting estimate of z_{oSF}. As expected, the results (Figure 14) show z_{oSF} systematically decreases as survey resolution is increased, with convergence to a scale-independent value at sampling intervals of less than ~0.01 m. It follows that z_{oSF} has been systematically underestimated for the Mekong riverbanks (since our sampling interval was 0.50 m). However, the prior sensitivity analyses (Figure 13d) show that bank erosion rate is likely unaffected by this error, due to the relatively insensitive response across the specific range of z_{oSF} values that are relevant in this case. The availability of historical (2005 and 2006) photogrammetric surveys from the Cecina study site also provides an opportunity to undertake a preliminary test of one of the key model assumptions (see section 6); namely that, at the scale of the reach, the derived bank roughness parameters remain time invariant, even when the bank is actively retreating. The data partially support this assumption. Statistical tests (ANOVA) reveal that the bump spacing (λ) values obtained for each survey date (2005, 2006, 2008) do not differ significantly (P = 0.346), but the estimated bump protrusion lengths, H, are significantly different (P < 0.001). The results for the streamwise length scale (σ) of each bump also provide some evidence of difference, even if the P value obtained (0.068) is not less than 0.05.

[55] The above discussion suggests that the most likely sources of error contributing to the evident overprediction of bank erosion rate in this study is either (1) systematic underestimation of the bank material erodibility parameters as obtained from the CSM, or (2) systematic overprediction of τ_{sf} due to the omission of secondary scales of bank form roughness. A final possibility is that the value of the exponent a in equation (1) is not equal to unity in this case. Further work is necessary to demonstrate whether either, or both, of a revised CSM calibration or the routine characterization of bank topography at finer spatial resolution would indeed lead to improved model fit.

6. Conclusion

[56] In this study a combination of analytical modeling and novel field measurement techniques is employed to parameterize an excess shear stress model of riverbank erosion, with the new model being applied to the fine-grained, cohesive, riverbanks of the Lower Mekong River.

Bank boundary shear stress is estimated using a model [*Kean and Smith*, 2006a, 2006b] of flow over the irregular bank topography that is characteristic of fine-grained riverbanks. The Kean and Smith model provides a means to partition the form and skin drag components of bank boundary shear stress and thus determine the extent to which form drag influences bank erosion rates. In addition, the use of the CSM enables bank material erodibility parameters to be estimated directly. The use of these two methods in tandem has enabled this study to present the very first predictions of hydraulic bank erosion rates that do not require recourse to calibration. This, together with the point that the form drag component of bank boundary shear stress has typically been neglected hitherto, significantly enhances the physical basis of the bank erosion model presented herein relative to prior studies.

[57] The main finding of this study concerns the dominance of the form drag component in the bank boundary shear stress partitioning. Specifically, form drag was found to accounts for between 61% (Ban Hom) and 85% (Pakse) of the total stress imparted on the riverbanks investigated in this study. This dominant form drag component has the effect of reducing the skin drag that actually drives bank erosion to values similar to the estimated critical shear stresses. As such, the presence of high bank form roughness, induced by the presence of irregular bank topography, can be viewed as a key factor that self-limits the rate of bank erosion.

[58] Preliminary results that suggest that the new model has a tendency to overpredict bank erosion rates notwithstanding, a lack of suitable data inhibited comprehensive model validation in this study. It is therefore appropriate to conclude by highlighting some of the key assumptions employed in the model's derivation.

[59] 1. The model does not directly consider how mass wasting, common along the high banks of the Mekong, influences bank top retreat. Rather, consistent with the concept of basal endpoint control [*Carson and Kirkby*, 1972; *Thorne*, 1982], it is assumed that parallel bank retreat occurs at a rate that is controlled by the rate of hydraulically forced bank toe erosion. The veracity of this assumption has been tested by undertaking trial simulations (not reported here) that follow *Rinaldi et al.* [2008] in coupling fluvial erosion (as simulated here), mass wasting and finite element seepage analyses, for a range of flow hydrographs. In these simulations rates of bank top retreat are virtually identical to rates of bank toe retreat at both Ang Nyay and Pakse.

[60] 2. In applying equation (1) it is assumed that the threshold shear stresses associated with the onset and cessation of hydraulic erosion are identical. Temporal variations in bank material erodibility associated with the effects of weathering and/or seasonal wetting/drying cycles have been documented in prior studies [*Prosser et al.*, 2000; *Couper and Maddock*, 2001; *Couper*, 2004; *Wynn et al.*, 2008], but are excluded from consideration here. Given the LMB's tropical climate, there is no doubt significant potential for effective subaerial weathering on exposed bank faces. Nevertheless, the focus in this study is on bank toe materials located at, near, or below the dry season waterline. It is therefore speculated that bank toe materials are less likely to experience the variations in thermal or moisture conditions that are necessary to induce significant time variations in erodibility.

[61] 3. It is assumed that any hysteresis in the relationship between flow discharge and outer region flow velocity, and thus in the relationship between flow discharge and boundary shear stress, is sufficiently small that there is no significant difference in the functions linking τ_{sf} to Q on the falling and rising limbs of the flow hydrograph. The presence or absence of hysteresis can only be explored at the Ang Nyay and Pakse study sites, where ADCP data are available. There is no evidence of hysteresis at Pakse (Figure 10d), but at Ang Nyay boundary shear stress values are significantly higher on the falling limb of the hydrograph (Figure 10a). This hysteresis is evidently forced by u_{out} values being higher on falling limb flows, probably due to the influence on the flow field of an island immediately upstream of the study site. Whatever the precise cause of the hysteresis at Ang Nyay, a lack of data at this site inhibits derivation of separate τ_{sf} versus Q relations (for use in equation 1) to better characterize rising limb and falling limb flows. For this reason the single function shown on Figure 10a is preferred for use in this study, noting that the consequent likely overprediction of instantaneous daily erosion rates on rising limb flows is probably offset by underprediction of instantaneous daily erosion rates on falling limb flows. Net errors in long-term erosion rates are, therefore, likely most pronounced in years when the flow hydrograph shape is distinctly asymmetric.

[62] 4. It is assumed that the relationship between flow discharge and outer region flow velocity, as might for example be caused by long-term morphological adjustments, remains invariant throughout the duration of model simulations.

[63] 5. It is assumed that bank roughness parameters remain time invariant. At any specific point on the bank profile this is clearly unlikely to be the case, as the process of bank erosion by definition must alter the bank morphology and thereby affect the local roughness. However, it remains unclear whether ongoing hydraulic erosion of a *sequence* of bumps would lead to systematic variations, random changes, or no changes at all, in the statistical properties (H_{reg}, σ_{reg}, λ_{reg}) of that sequence, the latter being the key data that are employed in the model simulations.

[64] These limitations notwithstanding, the new model developed here presents some clear practical advantages beyond its enhanced physical basis. Specifically, the excess shear stress model used to simulate bank erosion is very simple and can, by the simple expedient of establishing a relationship between flow discharge and bank boundary shear stress, be driven using estimates of flow discharge. Consequently, the new model offers the means to construct multidecadal time series of simulated bank erosion rates using readily available flow discharge records, which is useful for the purpose of examining hydro-climatological controls on bank erosion.

and Tess Wynn for their very helpful, thoughtful, and constructive reviews, which have contributed greatly to enhancing the clarity of the manuscript.

References

Aberle, J., V. Nikora, and R. Walters (2006), Data interpretation for in situ measurements of cohesive sediment erosion, *J. Hydraul. Eng.*, *132*, 581–588, doi:10.1061/(ASCE)0733-9429(2006)132:6(581).

Arulanandan, K., E. Gillogley, and R. Tully (1980), Development of a quantitative method to predict critical shear stress and rate of erosion of natural undisturbed cohesive soils, *Tech. Rep. GL-80-5*, U. S. Army Corps of Eng. Waterw. Exp. Stn., Vicksburg, Miss.

Black, K. S., and T. J. Tolhurst (2000), The Mk 4 60psi cohesive strength meter (CSM), user manual, Sediment Serv., Horsham, U. K.

Carling, P. A. (2009a), The geology of the Lower Mekong River, in *The Mekong: Biophysical Environment of an International River Basin*, pp. 13–28, edited by I. Campbell, Academic, New York.

Carling, P. A. (2009b), Geomorphology and sedimentology of the Lower Mekong River, in *The Mekong: Biophysical Environment of an International River Basin*, edited by I. Campbell, pp. 77–111, Academic, New York.

Carson, M. A., and M. J. Kirkby (1972), *Hillslope Form and Process*, Cambridge Univ. Press, Cambridge, U. K.

Clark, L. A., and T. M. Wynn (2007), Methods for determining streambank critical shear stress and soil erodibility: Implications for erosion rate predictions, *Trans. ASABE*, *50*, 95–106.

Constantine, C. R., T. Dunne, and G. J. Hanson (2009), Examining the physical meaning of the bank erosion coefficient used in meander migration modeling, *Geomorphology*, *106*, 242–252, doi:10.1016/j.geomorph. 2008.11.002.

Couper, P. (2004), Space and time in river bank erosion research: A review, *Area*, *36*, 387–403, doi:10.1111/j.0004-0894.2004.00239.x.

Couper, P., and I. P. Maddock (2001), Subaerial river bank erosion processes and their interaction with other bank erosion mechanisms on the River Arrow, Warwickshire, UK, *Earth Surf. Processes Landforms*, *26*, 631–646, doi:10.1002/esp.212.

Darby, S. E. (1998), River width adjustment II: Modeling, *J. Hydraul. Eng.*, *124*, 903–917.

Eaton, B. C., M. Church, and R. G. Millar (2004), Rational regime model of alluvial channel morphology and response, *Earth Surf. Processes Landforms*, *29*, 511–529, doi:10.1002/esp.1062.

Goodson, J. M., A. M. Gurnell, P. G. Angold, and I. P. Morrissey (2002), Riparian seed banks along the lower River Dove, UK: Their structure and ecological implications, *Geomorphology*, *47*, 45–60, doi:10.1016/S0169-555X(02)00140-X.

Govers, G. (1991), Rill erosion on arable land in central Belgium: Rates, controls and predictability, *Catena*, *18*, 133–155, doi:10.1016/0341-8162(91)90013-N.

Grissinger, E. H. (1982), Bank erosion of cohesive materials, in *Gravel-Bed Rivers*, edited by R. D. Hey, J. C. Bathurst, and C. R. Thorne, pp. 273–287, John Wiley, Chichester, U. K.

Gupta, A., and S. C. Liew (2007), The Mekong from satellite imagery: A quick look at a large river, *Geomorphology*, *85*, 259–274, doi:10.1016/j.geomorph.2006.03.036.

Hanson, G. J. (1990), Surface erodibility of earthen channels at high stresses. Part II: Developing an in situ testing device, *Trans. ASAE*, *33*, 132–137.

Hanson, G. J., and A. Simon (2001), Erodibility of cohesive streambeds in the loess area of the midwestern USA, *Hydrol. Processes*, *15*, 23–38, doi:10.1002/hyp.149.

Hooke, J. M. (1980), Magnitude and distribution of rates of river bank erosion, *Earth Surf. Processes Landforms*, *5*, 143–157.

Hopson, T. M. (1999), The form drag of large natural vegetation along the banks of open channels, M. S. thesis, 114 pp., Univ of Colo., Boulder.

Howard, A. D. (1994), Badlands, in *Geomorphology of Desert Environments*, edited by A. D. Abrahams and A. J. Parsons, pp. 213–242, Chapman and Hall, London.

Julian, J. P., and R. Torres (2006), Hydraulic erosion of cohesive riverbanks, *Geomorphology*, *76*, 193–206, doi:10.1016/j.geomorph.2005.11.003.

Kean, J. W. (2003), Computation of flow and boundary shear stress near the banks of streams and rivers, Ph.D. thesis, Univ of Colo., Boulder.

Kean, J. W., and J. D. Smith (2005), Generation and verification of theoretical rating curves in the Whitewater River basin, Kansas, *J. Geophys. Res.*, *110*, F04012, doi:10.1029/2004JF000250.

Kean, J. W., and J. D. Smith (2006a), Form drag in rivers due to small-scale natural topographic features: 1. Regular sequences, *J. Geophys. Res.*, *111*, F04009, doi:10.1029/2006JF000467.

Kean, J. W., and J. D. Smith (2006b), Form drag in rivers due to small-scale natural topographic features: 2. Irregular sequences, *J. Geophys. Res.*, *111*, F04010, doi:10.1029/2006JF000490.

Koponen, J., E. Alasaarela, K. Lehtinen, J. Sarkkula, P. Simbierowicz, H. Vepsä, and M. Virtanen (1992), Modelling the dynamics of a large sea area: Bothnian Bay Research Project 1988–90, *Publ. Water Environ. Res. Inst.*, *7*, 1–91.

Koponen, J., et al. (2008), Hydrological, environmental and socio-economic modelling tools for the Lower Mekong Basin impact assessment, *WUP-FIN Phase II Model Rep.*, 413 pp., Mekong River Comm., Vientiane, Laos. (Available at http://www.eia.fi/wup-fin/wup-fin2/publications.htm)

Kummu, M. (2008), Spatio-temporal scales of hydrological impact assessment in large river basins: The Mekong case, Ph.D. thesis, Water Resour. Res. Unit, Helsinki Univ. of Technol., Espoo, Finland. (Available at http://lib.tkk.fi/Diss/2008/isbn9789512296668/)

Kummu, M., X. X. Lu, A. Rasphone, J. Sarkkula, and J. Koponen (2008), Riverbank changes along the Mekong River: Remote sensing detection in the Vientiane-Nong Khai area, *Quaternary Int.*, *186*, 100–112, doi:10.1016/j.quaint.2007.10.015.

Liu, S., P. Lu, D. Liu, and P. Jin (2007), Pinpointing source of Mekong and measuring its length through analysis of satellite imagery and field investigations, *Geo-Spatial Inf. Sci.*, *10*(1), 51–56, doi:10.1007/s11806-007-0011-6.

Luppi, L., M. Rinaldi, L. B. Teruggi, S. E. Darby, and L. Nardi (2009), Monitoring and numerical modelling of riverbank erosion processes: A case study along the Cecina River (central Italy), *Earth Surf. Processes Landforms*, *34*, 530–546, doi:10.1002/esp.1754.

Marron, D. C. (1992), Floodplain storage of mine tailings in the Belle Fourche River, *Earth Surf. Processes Landforms*, *17*, 675–685, doi:10.1002/esp.3290170704.

McBride, M., W. C. Hession, D. M. Rizzo, and D. M. Thompson (2007), The influence of riparian vegetation on near-bank turbulence: A flume experiment, *Earth Surf. Processes Landforms*, *32*, 2019–2037, doi:10.1002/esp.1513.

McLean, S. R., and J. D. Smith (1986), A model for flow over two-dimensional bed forms, *J. Hydraul. Eng.*, *112*, 300–317, doi:10.1061/(ASCE)0733-9429(1986)112:4(300).

Mekong River Commission (1961), Hydrographic atlas of 1961 for the Mekong. surveyed in 1959–1961, Vientiane, Laos.

Mekong River Commission (1992), Hydrographic atlas of 1992 for the Mekong. surveyed in 1989–1992, Vientiane, Laos.

Mekong River Commission (2005), Overview of the hydrology of the Mekong River basin, Vientiane, Laos.

Millar, R. G. (2000), Influence of bank vegetation on alluvial channel patterns, *Water Resour. Res.*, *36*, 1109–1118, doi:10.1029/1999WR900346.

Milliman, J. D., and R. H. Meade (1983), World-wide delivery of river sediments to the oceans, *J. Geol.*, *91*, 1–21, doi:10.1086/628741.

Mosselman, E. (1998), Morphological modeling of rivers with erodible banks, *Hydrol. Processes*, *12*, 1357–1370, doi:10.1002/(SICI)1099-1085(19980630)12:8<1357::AID-HYP619>3.0.CO;2-7.

Osman, A. M., and C. R. Thorne (1988), Riverbank stability analysis. I: Theory, *J. Hydraul. Eng.*, *114*, 134–150, doi:10.1061/(ASCE)0733-9429(1988)114:2(134).

Partheniades, E. (1965), Erosion and deposition of cohesive soils, *J. Hydraul. Div. Am. Soc. Civ. Eng.*, *91*, 105–138.

Paterson, D. M. (1989), Short term changes in the erodibility of intertidal cohesive sediments related to the migratory behaviour of epipelic diatoms, *Limnol. Oceanogr.*, *34*(1), 223–234, doi:10.4319/lo.1989.34.1.0223.

Piégay, H., S. E. Darby, E. Mosselman, and N. Surian (2005), A review of techniques available for delimiting the erodible river corridor: A sustainable approach to managing bank erosion, *River Res. Appl.*, *21*, 773–789, doi:10.1002/rra.881.

Prosser, I. P., A. O. Hughes, and I. D. Rutherfurd (2000), Bank erosion of an incised upland channel by subaerial processes: Tasmania, Australia, *Earth Surf. Processes Landforms*, *25*, 1085–1101, doi:10.1002/1096-9837(200009)25:10<1085::AID-ESP118>3.0.CO;2-K.

Reneau, S. L., P. G. Drakos, D. Katzman, D. V. Malmon, E. V. McDonald, and R. T. Ryti (2004), Geomorphic controls on contaminant distribution along an ephemeral stream, *Earth Surf. Processes Landforms*, *29*, 1209–1223, doi:10.1002/esp.1085.

Rinaldi, M., and N. Casagli (1999), Stability of streambanks formed in partially saturated soils and effects of negative pore water pressures: The Sieve River (Italy), *Geomorphology*, *26*, 253–277, doi:10.1016/S0169-555X(98)00069-5.

Rinaldi, M., and S. E. Darby (2007), Modelling river-bank-erosion processes and mass failure mechanisms: Progress towards fully coupled simulations, in *Gravel-Bed Rivers 6: From Process Understanding to River Restoration*, *Dev. Earth Surf. Processes*, vol. 11, edited by H. Habersack, H. Piégay, and M. Rinaldi, pp. 213–239, Elsevier, Amsterdam, doi:10.1016/S0928-2025(07)11126-3.

Rinaldi, M., N. Casagli, S. Dapporto, and A. Gargini (2004), Monitoring and modeling of pore water pressure changes and riverbank stability during flow events, *Earth Surf. Processes Landforms*, *29*, 237–254, doi:10.1002/esp.1042.

Rinaldi, M., B. Mengoni, L. Luppi, S. E. Darby, and E. Mosselman (2008), Numerical simulation of hydrodynamics and bank erosion in a river bend, *Water Resour. Res.*, *44*, W09428, doi:10.1029/2008WR007008.

Samadi, A., E. Amiri-Tokaldany, and S. E. Darby (2009), Identifying the effects of parameter uncertainty on the reliability of riverbank stability modelling, *Geomorphology*, *106*, 219–230, doi:10.1016/j.geomorph.2008.10.019.

Schlichting, H. (1979), *Boundary-Layer Theory*, 817 pp., McGraw-Hill, New York.

Sen, P. K. (1968), Estimate of the regression coefficient based on Kendall's tau, *J. Am. Stat. Assoc.*, *63*, 1379–1389, doi:10.2307/2285891.

Simon, A., and A. J. Collison (2002), Quantifying the mechanical and hydrological effects of vegetation on streambank stability, *Earth Surf. Processes Landforms*, *27*, 527–546, doi:10.1002/esp.325.

Simons, T. J. (1980), Circulation models of lakes and inland seas, *Can. Bull. Fish. Aquat. Sci.*, *203*, 1–146.

Smith, J. D., and S. R. McLean (1977), Spatially averaged flow over a wavy surface, *J. Geophys. Res.*, *82*, 1735–1746, doi:10.1029/JC082i012p01735.

Theil, H. (1950), A rank-invariant method of linear and polynomial regression analysis, *Indagationes Math.*, *12*, 85–91.

Thieler, E. R., E. A. Himmelstoss, J. L. Zichichi, and A. Ergul (2009), Digital Shoreline Analysis System (DSAS) version 4.0—An ArcGIS extension for calculating shoreline change, *U. S. Geol. Surv. Open File Rep. 2008–1278*. (Available at http://pubs.usgs.gov/of/2008/1278/)

Thoman, R. W., and S. L. Niezgoda (2008), Determining erodibility, critical shear stress, and allowable discharge estimates for cohesive channels: Case study in the Powder River basin of Wyoming, *J. Hydrol. Eng.*, *134*, 1677–1687, doi:10.1061/(ASCE)0733-9429(2008)134:12(1677).

Thorne, C. R. (1982), Processes and mechanisms of river bank erosion, in *Gravel-Bed Rivers: Fluvial Processes, Engineering, and Management*, edited by R. D. Hey, J. C. Bathurst, and C. R. Thorne, pp. 227–271, John Wiley, Chichester, U. K.

Thorne, S. D., and D. J. Furbish (1995), Influences of coarse bank roughness on flow within a sharply curved river bend, *Geomorphology*, *12*, 241–257, doi:10.1016/0169-555X(95)00007-R.

Thorne, C. R., and J. Lewin (1979), Bank processes, bed-material movement and planform development in a meandering river, in *Adjustment of the Fluvial System*, edited by D. D. Rhodes and G. P. Williams, pp. 117–137, Kendall Hunt, Dubuque, Iowa.

Tolhurst, T. J., K. S. Black, S. A. Shayler, S. Mather, I. Black, K. Baker, and D. M. Paterson (1999), Measuring the in situ erosion shear stress of intertidal sediments with the cohesive strength meter (CSM), *Estuarine Coastal Shelf Sci.*, *49*, 281–294, doi:10.1006/ecss.1999.0512.

Tolhurst, T. J., K. S. Black, D. M. Paterson, H. J. Mitchener, G. R. Termaat, and S. A. Shayler (2000), A comparison and measurement standardization of four in situ devices for determining the erosion shear stress of intertidal sediments, *Cont. Shelf Res.*, *20*, 1397–1418, doi:10.1016/S0278-4343(00)00029-7.

Vardy, S., J. E. Saunders, T. J. Tolhurst, P. A. Davies, and D. M. Paterson (2007), Calibration of the high-pressure cohesive strength meter (CSM), *Cont. Shelf Res.*, *27*, 1190–1199, doi:10.1016/j.csr.2006.01.022.

Virtanen, M., J. Koponen, K. Dahlbo, and J. Sarkkula (1986), Three-dimensional water-quality–transport model compared with field observations, *Ecol. Modell.*, *31*, 185–199, doi:10.1016/0304-3800(86)90063-3.

Whiting, P. J., and W. E. Dietrich (1990), Boundary shear stress and roughness over mobile alluvial beds, *J. Hydraul. Eng.*, *116*, 1495–1511, doi:10.1061/(ASCE)0733-9429(1990)116:12(1495).

Wiberg, P. L., and J. D. Smith (1991), Velocity distribution and bed roughness in steep streams, *Water Resour. Res.*, *27*, 825–838, doi:10.1029/90WR02770.

Widdows, J., P. L. Friend, A. J. Bale, M. D. Brinsley, N. D. Pope, and C. E. L. Thompson (2007), Inter-comparison between five devices for determining erodibility of intertidal sediments, *Cont. Shelf Res.*, *27*, 1174–1189, doi:10.1016/j.csr.2005.10.006.

Wynn, T. M., M. B. Henderson, and D. H. Vaughan (2008), Changes in streambank erodibility and critical shear stress due to subaerial processes along a headwater stream, southwestern Virginia, USA, *Geomorphology*, *97*, 260–273, doi:10.1016/j.geomorph.2007.08.010.

P. A. Carling, S. E. Darby, J. Leyland, and H. Q. Trieu, School of Geography, University of Southampton, Highfield, Southampton SO17 1BJ, UK. (s.e.darby@soton.ac.uk)

I. Conlan, Department of Resource Management and Geography, University of Melbourne, Melbourne, Vic 2010, Australia.

J. Koponen, Environmental Impact Assessment Centre of Finland Ltd, Tekniikantie 21b, Espoo FI-02150, Finland.

M. Kummu, Water and Development Research Group, Aalto University School of Science and Technology (TKK), Aalto University, Espoo FIN-02015, Finland.

J. Sarkkula, Finnish Environment Institute, P.O. Box 140, Helsinki FI-00251, Finland.